

# Neonatal immunity associated with heterologous HIV-1 neutralizing antibody induction in SHIV-infected Rhesus Macaques

---

Received: 23 February 2024

---

Accepted: 20 November 2024


---

Published online: 27 November 2024

---

 Check for updates

---

Sommer Holmes<sup>1,13</sup>, Hui Li<sup>2,13</sup>, Xiaoying Shen<sup>3,13</sup>, Mitchell Martin<sup>1,13</sup>, Ryan Tuck<sup>1,13</sup>, Yue Chen<sup>1,13</sup>, Elena E. Giorgi<sup>4</sup>, H       Fradin Kirshner<sup>1</sup>, Madison Berry<sup>1</sup>, Elizabeth Van Italie<sup>1</sup>, Sravani Venkatayogi<sup>1</sup>, Joshua S. Martin Beem<sup>1</sup>, Robert J. Edwards<sup>1</sup>, Katayoun Mansouri<sup>1</sup>, Ajay Singh<sup>2</sup>, Cindy Kuykendall<sup>1</sup>, Thaddeus Gurley<sup>1</sup>, M. Anthony Moody<sup>1,5,6</sup>, Nicole DeNayer<sup>1</sup>, Todd Demarco<sup>1</sup>, Thomas N. Denny<sup>1,7</sup>, Yunfei Wang<sup>1</sup>, Tyler D. Evangelous<sup>1</sup>, John T. Clinton<sup>1</sup>, Bhavna Hora<sup>1</sup>, Kshitij Wagh<sup>8</sup>, Michael S. Seaman<sup>9</sup>, Kevin O. Saunders<sup>1,3,5,10</sup>, Nicholas Solomotis<sup>11</sup>, Johnathan Misamore<sup>11</sup>, Mark G. Lewis<sup>11</sup>, Kevin Wiehe<sup>1,12</sup>, David C. Montefiori<sup>1,3</sup>, George M. Shaw<sup>2</sup> & Wilton B. Williams<sup>1,3,5</sup> 

The details of the pediatric immune system that supports induction of antibodies capable of neutralizing geographically-diverse or heterologous HIV-1 is currently unclear. Here we explore the pediatric immune environment in neonatal macaque undergoing Simian-HIV infection. Simian-HIV infection of 11 pairs of therapy-na  ve dams and infant rhesus macaques for 24 months results in heterologous HIV-1 neutralizing antibodies in 64% of young macaques compared to 18% of adult macaques. Heterologous HIV-1 neutralizing antibodies emerge by 12 months post-infection in young macaques, in association with lower expression of immunosuppressive genes, fewer germinal center CD4 + T regulatory cells, and a lower ratio of CD4 + T follicular regulatory to helper cells. Antibodies from peripheral blood B cells in two young macaques following SHIV infection neutralize 13% of 119 heterologous HIV-1 strains and map to regions of canonical broadly neutralizing antibody epitopes on the envelope surface protein. Here we show that pediatric immunity to SHIV infection in a macaque model may inform vaccine strategies to induce effective HIV-1 neutralizing antibodies in infants and children prior to viral exposure.

The immune cell subsets in human infants and adults have quantitative and qualitative differences<sup>1–3</sup>, but infants possess B and T cells capable of responding to pathogens and immunogens<sup>4–6</sup>. In both humans and non-human primates (NHPs), infants can mount some immune responses similarly to adults<sup>4,7,8</sup> as well as generate effective antigen-specific responses to vaccine immunogens<sup>8–11</sup>. These studies highlight the potential for early-life immunity when harnessed via vaccines to respond to pathogens.

A key goal of a HIV-1 vaccine is to elicit broadly neutralizing antibodies (bnAbs) that target conserved epitopes on the viral-surface envelope (Env) protein<sup>12–15</sup>. HIV-1 Env bnAbs develop in ~50% of people living with HIV-1 (PLWH) after 3–5 years of infection<sup>16</sup>, but infants and children PLWH have been reported to more frequently develop bnAbs and do so faster than adults<sup>7,17</sup>. From one bnAb-generating infant (BF520)<sup>17</sup>, a bnAb targeting the Env V3-glycan bnAb epitope was found that had a less mutated heavy chain gene when compared to bnAbs

isolated from chronically-infected HIV-1 adults<sup>18</sup>, suggesting that infants may have an alternate or accelerated pathway to bnAb development. However, the mechanisms for bnAb induction in infants and children are not fully defined, and studies comparing B cell repertoires that shape antibody responses, including bnAb induction in infant and adult populations, are lacking.

Lymph node (LN)-derived germinal centers (GCs) are anatomical sites of B-cell proliferation, somatic hypermutation (SHM), and class-switch recombination, and are the source of memory B cells and long-lived plasma cells that generate effective antibody responses to pathogens and immunogens<sup>19,20</sup>. In adult humans and NHPs, a key correlate of bnAb induction is the ratio of CD4<sup>+</sup> T follicular regulatory (TFR) to helper (TFH) cell subsets in LN-derived GCs<sup>21–23</sup>. GC TFH cells can stimulate B cells to mature during bnAb development, whereas TFR cells can suppress TFH cell and B-cell activity thus limiting bnAb development<sup>21,24,25</sup>. However, GC immune cell subsets and their functions related to bnAb induction in infants and children are understudied.

The recent development of transmitted-founder (TF) Env SHIV infection of rhesus macaques (RMs) provided a model that can be employed to further our understanding of the cellular and molecular correlates of bnAb induction<sup>26–28</sup>. We adapted this SHIV infection model from Roark and colleagues<sup>28</sup> in neonate RMs where neonatal SHIV infection elicited heterologous HIV-1 NAb with characteristics of bnAbs<sup>29,30</sup>. Moreover, our neonatal SHIV-infection model in RMs displayed properties that mimicked human HIV-1 infection as described<sup>29</sup>, thus providing an appropriate model to interrogate the mechanisms of host immunity that support bnAb induction in early-life.

In this study, we evaluated host and viral factors in response to the same SHIV in pairs of dams and infant RMs as surrogates for adult and infant populations. Therapy-naïve SHIV-infected neonate and dam RMs had differences in humoral immunity over time, including induction of heterologous HIV-1 NAb following SHIV infection in more of the neonate RMs compared to adult dams. Peripheral blood B cell-derived monoclonal antibodies (mAbs) from two representative young RMs demonstrated limited heterologous HIV-1 neutralizing activity similar to plasma HIV-1 NAb. Phenotypic characterization of LN-derived immune cells along with RNA-sequencing (seq) gene expression analysis (GEX) demonstrated that young RMs had a less immunosuppressive GC environment that was permissive for heterologous HIV-1 NAb induction compared to adult RMs. Additionally, we evaluated the B cell receptor (BCR) repertoires used by neonate and dam RMs following SHIV infection, and defined genetic signatures in Env during viral evolution that may contribute to the initiation and maturation of HIV-1 neutralizing B cell lineages in neonate RMs. Here, we demonstrated cellular and molecular mechanisms of heterologous HIV-1 NAb induction in a pediatric model of macaque SHIV infection that may be harnessed by appropriate vaccine strategies.

## Results

### Neonatal and adult SHIV infection

We studied 22 neonate and adult RMs infected with the same SHIV that was previously described<sup>29,30</sup>. In brief, all 22 RMs were challenged (see methods) with a highly infectious SHIV bearing HIV-1 Env CH848 10.17 DT.E169K that was sensitive to neutralization by bnAb lineages targeting NAb-epitopes in HIV-1 Env V2 and V3 regions<sup>29,30</sup> (Fig. 1A). Twenty of 22 RMs required 50 ng of p27 SHIV to achieve infection (Fig. 1B), in agreement with the challenge dose used to establish infection of adult RMs by other highly infectious and pathogenic SHIVs<sup>26–28</sup>. Two additional RMs were successfully infected with different SHIV doses (see methods). Both neonate and adult RMs had similar viral peak soon after challenge (Fig. 1C) that was consistent with previous studies of different pathogenic SHIVs in RMs<sup>26,27,31</sup>. However, over

the entire follow up time, young RMs had overall statistically significantly higher viral loads compared to adult RMs (measured as area under the curve of the log-transformed viral loads,  $p = 0.001$  2-sided by paired Wilcoxon test) (Fig. S1). These data implied that neonate and adult RMs have distinct host immunological factors that impact viremia control or persistence, which in turn may impact host immunity. Persistent high viremia was associated with induction of HIV-1 NAb following SHIV infection<sup>29,31</sup> and bnAb induction in human HIV-1 infection<sup>32</sup>, suggesting that persistent viremia contributes to the quality of antibody responses, in part due to continual antigen selection of BCRs for affinity maturation and development of b/NAb<sup>15</sup>. However, previous studies of infant and adult SHIV-infected RMs demonstrated that high plasma viremia alone was insufficient to elicit heterologous HIV-1 neutralization activity<sup>28,31</sup>. Thus, we sought to understand differences in host immunity to SHIV infection in neonate and adult RMs that were not limited to levels of viremia. Here, we evaluated host and viral factors associated with macaque SHIV infection collectively in the group of neonate RMs compared to the group of adult RMs to better understand potential mechanisms of neonatal immunity that may be harnessed by future HIV-1 vaccination. First, we compared the magnitudes and qualities of antibody responses elicited by the same SHIV in both neonate and adult RM populations.

### HIV-1 Env-reactive plasma antibodies

Longitudinal plasma antibodies from young (following neonatal SHIV infection) and adult RMs bound recombinant HIV-1 proteins, including autologous CH848 10.17 DT.E169K soluble stabilized trimer (SOSIP) and monomeric gp120 Envs, and heterologous V2-peptides, V3-peptide and gp41 oligomer, with varied magnitudes (Figs. 2A and S2). At the first time point following neonatal SHIV infection (–M5–8) (Fig. 2A), the magnitudes of plasma binding antibodies against the autologous HIV-1 Env proteins were statistically significantly higher than plasma binding antibodies generated in adult SHIV infection ( $p = 0.001$ , 2-way paired Wilcoxon test), and the comparison remained significant also after adjusting for the animals' viral loads ( $p = 3.7 \times 10^{-7}$  and 0.009 for autologous SOSIP and gp120, respectively, by ANOVA test). However, by the last time point available (M22–24) (Fig. 2A), neither comparison was significant ( $p = 0.76$  and 0.99 respectively, 2-way paired Wilcoxon test). Stabilized SOSIP trimers present some NAb epitopes that are not present on gp120 monomers, and majority of non-NAb epitopes present on gp120 are not exposed on the stabilized SOSIP trimer. Thus, that the magnitude of autologous SOSIP-reactive antibodies appeared to decrease over time in contrast with autologous monomer-reactive antibodies in both young and adult RMs (Fig. 2A) was suggestive of differences in the dynamics of antibody quality over time. In 5/11 neonate/dam pairs (V059/BJ56; V095/V056; V250/V151; V252/V154; and V253/V152), the adult RMs generated higher plasma binding antibodies across multiple timepoints against 2–5 heterologous V2-peptides (Fig. S2A) that are the targets of linear V2-reactive antibodies and a few bnAbs (Fig. S2B)<sup>33–35</sup>. As shown in Fig. S2B, linear V2-targeted non-NAb and CH01 or PG9 bnAbs bound V2 epitopes, thus we cannot rule out the induction of either type of Env V2-targeted antibodies in the plasma of SHIV-infected neonate and adult RMs. In competition ELISAs, plasma antibodies from all young RMs demonstrated similar or higher levels of blocking against reference V2-apex bnAb PG9<sup>36</sup> (Fig. S3A) as well as GDIR-targeted V3-glycan bnAb DH270<sup>37</sup> (Fig. S3B). These data indicated that plasma NAb in young and adult RMs in part may target bnAb epitopes in Env V2 and V3 regions (Figs. S2 and S3), but we cannot rule out competition by antibodies targeting neighboring regions on Env. Taken together, the plasma binding antibody profiles suggested that neonatal SHIV infection elicited similar or better-quality antibodies against HIV-1 Env compared to adult SHIV infection. Thus, we next evaluated the quality of SHIV-induced plasma antibodies in neonatal and adult SHIV infection by testing their neutralization capacities.

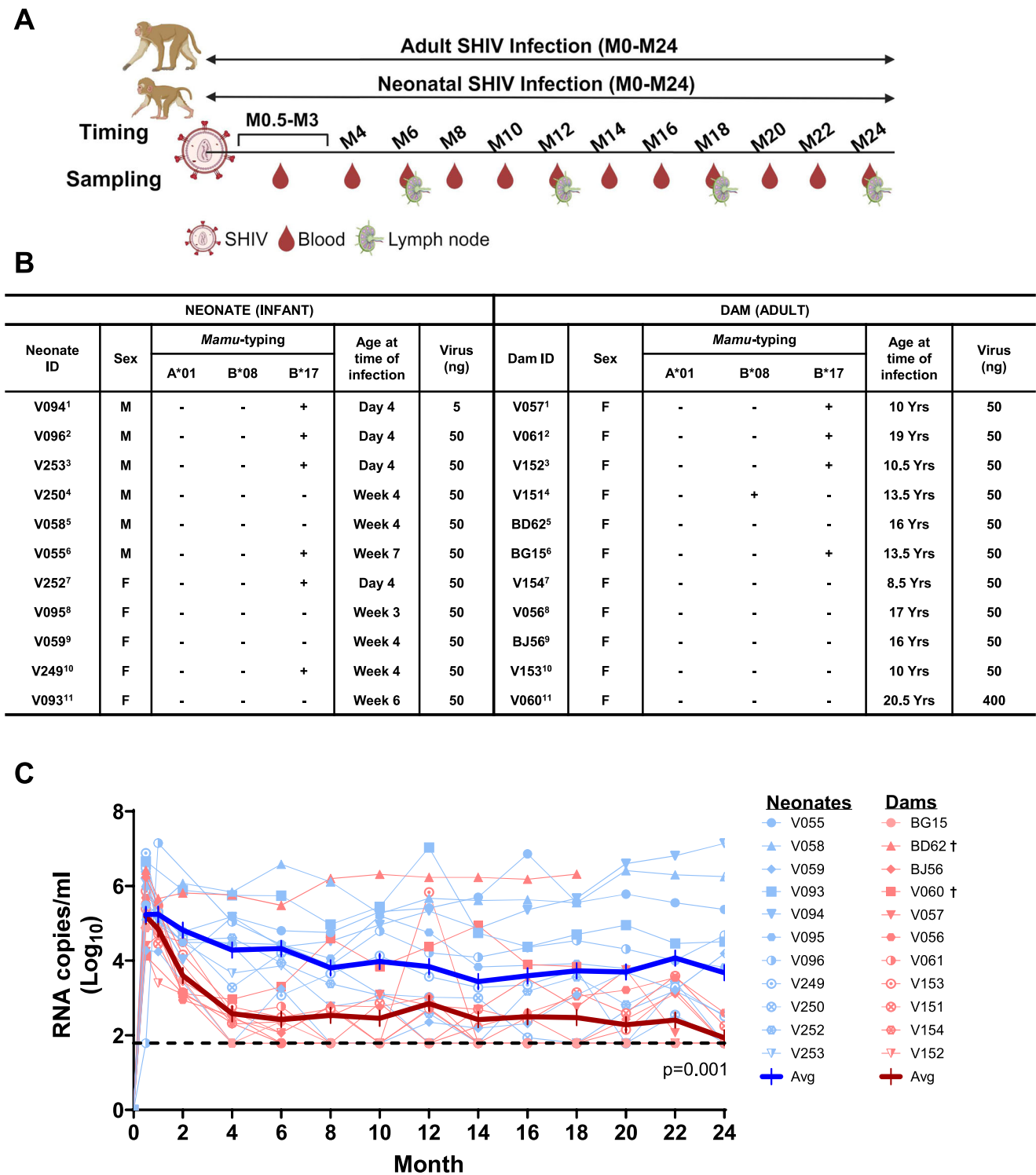


**Fig. 1 | Study design and viral dynamics.** **A** Sampling timeline following neonatal and adult SHIV-infection in 11 pairs of neonate and dam rhesus macaques (RMs). Peripheral blood (bi-monthly) and lymph node tissue sections (6-month intervals) were collected over time as shown. The sampling within the first 4 months of SHIV challenge varied across animals due to technical and biological variables. This figure panel was Created in BioRender. Williams, W. (2020) <https://BioRender.com/d04z220>. **B** Information on the neonate and adult RMs studied including their sex, genotype for SIV restrictive *Mamu*-alleles [negative (–) and positive (+)], and viral inoculum (ng P27) used to establish infection at the indicated age. Yrs is abbreviation for years for age of adult RMs, whereas age of neonate RMs at time of infection was reported in days or weeks post-birth. **C** Plasma viral load dynamics measured via qPCR and reported as SIV gag RNA copies/ml (Log<sub>10</sub>). Each symbol

represents an individual RM, but matching symbols represent each corresponding neonate (blue) and dam (red) pair. Longitudinal viral load levels per RM were connected by blue lines for neonate RMs and red lines for adult RMs. The thick blue and red lines represent the geometric mean of viral loads per timepoint for neonate and adult RMs, respectively. The horizontal dash line represents the limit of detection of the assay (1.79 RNA copies/ml). BD62 and V060 died (†) between 18–19 months post SHIV infection. For graphical purposes, some approximated timepoints were used for V057, V058 and V060; Source data are provided as a Source Data file. The reported p-value compares the log viral load area under the curve for adult-dam RMs ( $N=11$ ) compared to neonates ( $N=11$ ) using a 2-way paired Wilcoxon test.

### HIV-1 neutralization profile of plasma antibodies

Autologous plasma HIV-1 NAbS were generated in all young and adult RMs with neutralization titers decreasing over time from month 6 to 24 (Fig. 2B), suggestive of viral escape that eludes NAbS. We previously reported that autologous plasma NAbS were generated as early as 2–3 months post-infection in neonatal SHIV infection<sup>29</sup> in agreement with the detection of autologous plasma NAbS 1–2 months following adult SHIV infection (Table S1). Additionally, we previously reported that autologous plasma NAbS predominantly targeted V1-glycan hole, especially within 6 months of infection, following neonatal SHIV infection<sup>29</sup>, in agreement with autologous plasma NAbS elicited in adult SHIV infection (Fig. 2B). We used differences in magnitude of plasma NAb titers against autologous SHIV CH848 10.17 strains without (DT.E169K) and with (E169K) V1-glycans to assess neutralization epitope mapping. Interestingly, we also found that at all time points neonatal SHIV infection elicited higher geometric mean titers of plasma NAbS against SHIV CH848 10.17 E169K (+V1 glycans) compared to adult SHIV infection, but this trend was not statistically significant ( $p > 0.2$  for all tests) (Fig. 2B). That the neonates seemed to have higher titers of plasma NAbS against SHIV CH848 10.17 E169K lacking V1 glycans (Fig. 2B) implied differences in the quality of NAbS elicited by neonates and dams, given that antibodies that target glycan holes on Env have been postulated to be strain-specific and difficult to mature to breadth for neutralization of heterologous HIV-1 strains<sup>38,39</sup>.

Next, we tested plasma antibodies for neutralization of 14 heterologous HIV-1 strains, including difficult-to-neutralize or tier 2 primary isolates in the HIV-1 global reference panel<sup>40</sup> or viruses that showed a propensity to be neutralized by bnAbS targeting epitopes in the Env V2 and V3 regions<sup>28,41</sup> (Fig. 3, Table S2). We previously reported the neutralization profile of longitudinal plasma antibodies elicited by neonatal SHIV infection against this panel of 14 viruses<sup>29</sup>, and now report the neutralization profile of longitudinal plasma antibodies elicited by the same SHIV in adult RMs against the same panel of viruses. We found that neonatal SHIV infection preferentially elicited heterologous HIV-1 NAbS indicative of affinity maturation compared to adult SHIV infection (Fig. 3, Table S2). We previously defined induction of heterologous plasma NAbS in neonatal SHIV infection as plasma NAb titers indicative of affinity maturation with increasing titers over time against  $\geq 1$  heterologous HIV-1 strain or had persistent similar neutralization titers over time against  $\geq 2$  heterologous tier 2 HIV-1 strains<sup>29</sup>. Using this stringent criterion, we found that 7/11 (64%) neonate (Fig. 3A–G) versus 2/11 (18%) (Fig. 3A, B) adult SHIV-infected RMs generated heterologous HIV-1 NAbS ( $p = 0.08$ , Fisher's Exact Test).

### Heterologous HIV-1 neutralizing mAbS isolated from peripheral blood-derived B cells in neonatal SHIV infection

We next isolated and characterized mAbS from B cells among peripheral blood cells (PBMCs) in two representative RMs, V093 (Fig. 3A) and V055 (Fig. 3C), which were representative of young RMs with the best plasma heterologous HIV-1 neutralization titers. We used an antigen-specific high-throughput platform referred to as barcode-enable antigen mapping for B cells (BEAM-Ab) from 10X Genomics (Pleasanton, CA) in our pipeline for isolation and characterization of HIV-1 Env-reactive mAbS (Fig. 4A). We initially established our criteria for BEAM-Ab prediction matrices that were consistent with IgG antibody binding when the predicted HIV-1 Env-reactive BCR was recombinantly expressed as a mAb and tested for binding in ELISA (see methods) (Fig. S4A). From 16,982 recovered B cell receptors (BCRs) in V093 and V055 RMs, we identified 8 (0.05%) BCRs with predicted BEAM antigen-reactivity scores that met our selection criteria for binding at least one of five HIV-1 Env SOSIP trimers, but did not bind a non-HIV protein, which were used as B cell baits in BEAM-Ab (Fig. 4B). Six of eight (75%) mAbS with predicted HIV-1 Env-reactive BCRs bound to at least one HIV-1 Env trimer tested to which it was predicted to bind (Fig. 4B, C). Three mAbS, DH1518.1, DH1518.2, and DH1523, bound

multiple recombinant HIV-1 Env SOSIP trimers associated with heterologous tier 2 HIV-1 strains present in the global panel<sup>40</sup> (Fig. 4C and S4B). Clonally-related DH1518.1 and DH1518.2 had similar V(D)J rearrangements using VH4 genes with  $>80\%$  HCDR3 sequence identity and identical HCDR3 length of 17 amino acids, and both antibodies used the same VK2 gene. DH1523 used macaque VH7 gene with 15aa long HCDR3 that was paired with a VL1 gene.

Next, we used negative stain electron microscopy (NSEM) to visualize DH1518 IgG mAbS in complex with heterologous HIV-1 T250 SOSIP trimer (Figs. 4D and S5). We found that the two fragment antigen-binding (Fab) arms of a single IgG from DH1518.1 or DH1518.2 bound the two protomers of the trimer as the tops of the Fabs point towards each other (Fig. S5A). Given this arrangement, the two Fabs per IgG showed different approach angles as seen when they were superimposed onto a single protomer (Fig. S5B). We also observed a gap between the Fab and the trimer surface in each complex (Figure S5). These data suggested that these mAbS bound an extended and flexible epitope and possible rearrangement (or distortion) of the trimer apex. Future higher resolution structural analyses will fully define the epitope footprint of DH1518.1 and DH1518.2. Additionally, we found that recombinant HIV-1 Env binding by DH1518.1 and DH1518.2 was not outcompeted by 1M D-mannose (Fig. S4C), suggesting that these mAbS were not targeting individual glycans on HIV-1 Env, but we cannot rule out that they bind glycan clusters present on HIV-1 Env.

Interestingly, DH1518.1, DH1518.2 and DH1523 demonstrated varied neutralization potencies against 2–4 HIV-1 strains among the global panel of reference HIV-1 strains (Fig. 4E, F; Table S3). DH1518.1 had the best potency with up to 90% neutralization of viral particles against heterologous tier 2 HIV-1 strains X1632 and 25710 (Fig. 4E, Table S3). Both DH1518.1 and DH1518.2 neutralized  $\sim 13\%$  of a panel of 119 multi-clade or geographically-diverse heterologous tier 2 HIV-1 strains (Table S4), which includes viruses from the global panel<sup>40</sup> and are commonly used to assess neutralization breadth of HIV-1 Env-reactive bnAbS<sup>42</sup>; DH1518.1 and DH1518.2 had geometric mean neutralization titers with 50% inhibitory concentration (IC50) of 8.4 and 11  $\mu\text{g/ml}$ , respectively (Fig. 4F, Table S4). Additionally, we found that both DH1518.1 and DH1518.2 had 3–10 fold increase in neutralization titers against heterologous tier 2 HIV-1 25170 with a disruption of V2-apex, V3-glycan and CD4-binding site (BS) bnAb epitopes including removal of potential N-linked glycosylation sites (PNGS) at Env positions 160 (N160K) and 332 (N33A), respectively (Fig. 4G); this neutralization profile of DH1518 antibodies was consistent with plasma NAb mapping previously reported in these young RMs following neonatal SHIV infection<sup>29</sup>. Disruption of the V2-apex, V3-glycan and CD4BS bnAb epitopes on additional HIV-1 Env strains also increased neutralization susceptibility by DH1518.1 and DH1518.2 (Fig. 4G). Thus, these data raised the hypothesis that neonatal SHIV infection elicited NAbS such as DH1518.1 and DH1518.2 that mapped to bnAb epitopes, some of which may be partially occluded by glycans, and these mAbS had in part developed to accommodate these glycans by neutralizing the wild-type HIV-1 strains with the glycans intact. Despite limited neutralization breadth compared to best-in-class bnAbS<sup>43</sup>, these data suggested that heterologous HIV-1 neutralizing DH1518 B cell lineage that target bnAb epitopes may be able to develop over time with improved breadth; a goal for HIV-1 vaccines to recapitulate in pediatric populations prior to sexual debut.

### Germinal center dynamics in heterologous HIV-1 NAb induction

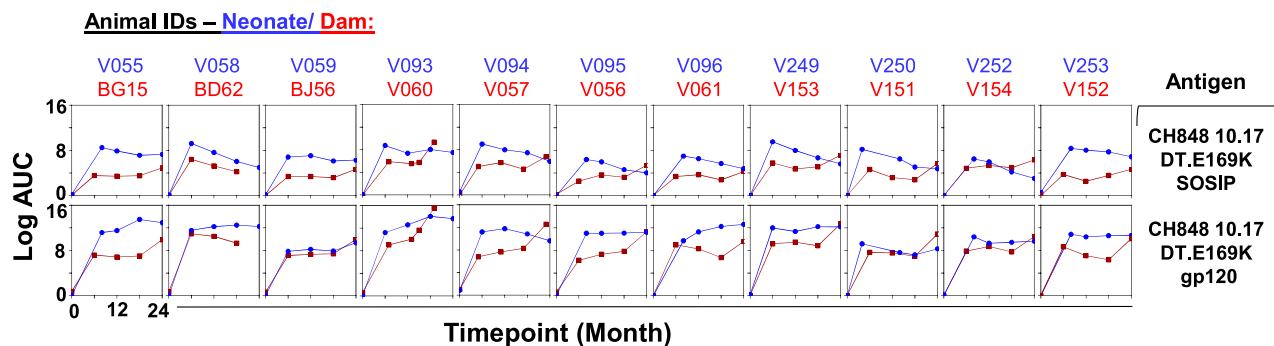
Previous studies in PLWH including adults<sup>21,44,45</sup> and children<sup>46</sup>, and NHPs<sup>29</sup>, indicated that extensive GC activity during SHIV infection drives antibody maturation and the acquisition of heterologous HIV-1 neutralization breadth that leads to bnAb development. We interrogated the immune cell subsets in LN-derived GCs over time following neonatal and adult SHIV infection in a subset of RMs in order to define immunological mechanisms associated with preferential heterologous



HIV-1 NAb induction in the younger animals. Here, we studied five neonate and dam pairs of RMs ( $N=10$ ) that all generated autologous tier 2 SHIV NAb, but 4/5 neonate (V055, V058, V094, and V095), and 1/5 adult (BD62), SHIV-infected RMs generated heterologous tier 2 HIV-1 NAb (Fig. 3, Table S2). Therefore, the 10 animals studied were representative of young and adult RMs with plasma HIV-1 NAb, and were also animals from which we had multiple vials of LN cells for future validation assays.

Since heterologous HIV-1 plasma NAb emerged by ~12 months or earlier in neonatal SHIV infection (Fig. 3), we compared the frequencies of LN-derived B and T cell subsets at this timepoint in the five neonate and dam pairs via flow cytometry (Figs. 5 and S6). We did not detect significant differences in B cell subsets, including antigen-reactive B cells, in neonatal and adult SHIV infections (Figs. 5A, B, S6A). Resting B cells constituted the highest proportion of LN B cells in both neonate and adult SHIV-infected RMs (Fig. 5A), while antigen-reactive B cells

### A. Binding to Autologous Envs



### B. Autologous SHIV Neutralization

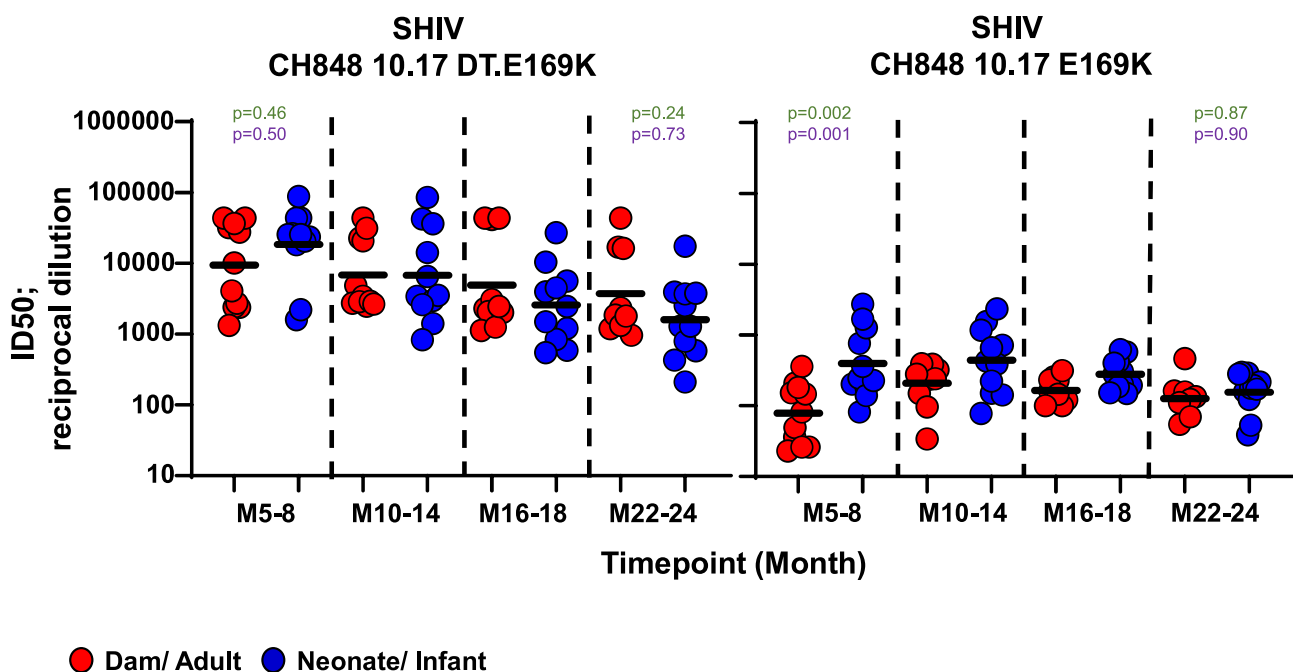


**Fig. 2 | Magnitudes and specificities of autologous HIV-1 Env-reactive binding and neutralizing antibodies elicited by neonate and adult SHIV infection.**

A Longitudinal plasma spanning 24 months post neonate and adult SHIV infection in RMs were tested for binding autologous (CH848 10.17 DT.E169K) SOSIP trimer and gp120 monomer. Binding was measured in ELISA and the binding titers were reported as Log AUC. Data shown represent average binding log AUC titers of 2-3 biological replicates. Blue line represents plasma binding antibody responses in SHIV-infected neonate RMs, whereas the red line represents plasma binding antibody responses in SHIV-infected adult RMs. At the first time point, plasma binding antibody responses in SHIV-infected neonate RMs ( $N=11$ ) were statistically significantly higher than plasma binding antibody responses in SHIV-infected adult RMs ( $N=11$ ) for both the autologous SOSIP and the gp120 monomer ( $p=0.001$  in both cases by 2-way paired Wilcoxon test, and  $p=3.7 \times 10^{-7}$  and  $0.009$  via ANOVA test from fitting a viral load adjusted generalized linear model). The same tests at the last time point yielded not significant  $p$ -values ( $p=0.76$  and  $0.99$  for trimer and

monomer, respectively, by 2-way paired Wilcoxon test; and  $p=0.77$  and  $0.63$  via ANOVA test for trimer and monomer, respectively). See control mAb binding in Figure S2. Due to limited sample availability in neonate RMs, plasma from HIV-1 negative dams (prior to SHIV infection) corresponding to each neonate RM was used as month 0 samples in ELISAs. B Longitudinal plasma antibodies elicited in neonatal (blue) and adult (red) SHIV infection were tested for neutralization of autologous SHIV CH848 10.17 DT.E169K [–V1 glycans] (left panel) and CH848 10.17 E169K [+V1 glycans] (right panel) in TZM-bl cells in a single experiment. Neutralization titer was measured as Log ID50 (reciprocal dilution) and horizontal bars indicate geometric means. Each symbol represents a different animal. To maximize sample availability per animal, we tested samples within intervals of 5–6, 10–14 and 16–18 months post-SHIV infection. Comparisons at first and last time point between neonate ( $N=11$ ) and dam-adult ( $N=11$ ) titers were obtained from 2-way paired Wilcoxon test (green) and ANOVA test from fitting viral-load adjusted generalized linear models (purple). A, B Source data are provided as a Source Data file.

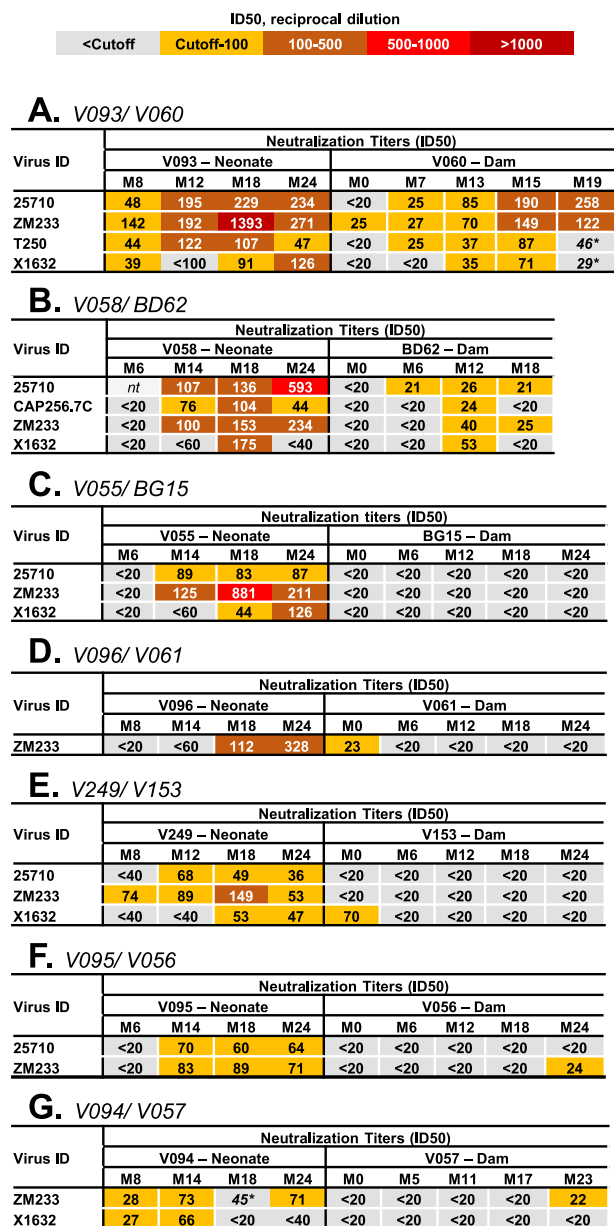


**Fig. 3 | Heterologous HIV-1 neutralization profile of plasma antibodies elicited by neonatal and adult SHIV infection. A–G** Longitudinal plasma antibodies spanning 24 months following neonatal and adult SHIV infection were tested for neutralization of heterologous HIV-1 reference strains from the global panel. Neutralization titer was measured in TZM-bl cells and reported as ID50 (reciprocal dilution). The heatmaps show the neutralization titers of plasma antibodies in seven young RMs with induction of heterologous HIV-1 NAb following neonatal SHIV infection (A–G), and their corresponding dams including two adult RMs with induction of heterologous HIV-1 NAb (A–B). See methods for criteria of heterologous HIV-1 NAb induction as described<sup>29</sup>. Shown are titers against viruses neutralized by the plasma samples that met our criteria for the induction of heterologous HIV-1 NAb induction. As shown by the key at the top of the figure, the heatmap was color coded to show the magnitude of NAb titers generated in each animal at different timepoints against each virus tested. Adults V060 and BD62 died before month 24 post-SHIV infection. Asterisk (\*); neutralization titer was less than 3X the negative control virus (MuLV).

were detected across the three LN B cell subsets analyzed (Fig. 5B). In terms of LN-derived CD4+ T cell subsets, SHIV-infected neonate RMs had a significantly ( $p$ -value < 0.05; Mann–Whitney Test) higher frequency of naïve CD4+ T cells compared with SHIV-infected adult RMs and the reverse was true for memory CD4+ T cells (Fig. 5C), in agreement with age-dependent differences of these immune cell

subsets<sup>3,47</sup>. Interestingly, within total LN lymphocytes of neonate and adult SHIV-infected RMs, memory TFH cells showed similar geometric means (Fig. S6B). However, CD4+ Treg cells expressing the forkhead box P3 (FOXP3) transcription factor (Fig. S6B), were higher in adults than in neonates, nearly reaching statistical significance ( $p$ -value = 0.0556; Mann–Whitney Test) (Fig. 5D). LN Tregs were consistently higher in adults for each neonate and adult-dam pair, and increased from approximately month 6 to 12 post SHIV-infection in 4/5 adult RMs (Fig. S7D), suggestive of host immunity to SHIV infection.

TFR cells present among Tregs in LNs<sup>23,48</sup> (Figs. 5E and S6B) hone to GCs and can limit TFH numbers and function<sup>49–52</sup>. The relative frequencies of TFR and TFH cells among GC CD4+ T cells, rather than TFR cell counts have been postulated to control GC B cell responses<sup>21,23,52</sup>. We found that both young and adult RMs at ~12 months post-infection had similar levels of TFH and TFR cells within LN lymphocytes (Fig. 5F), but young RMs had a lower ratio of the frequencies of TFR to TFH among LN lymphocytes (Fig. 5G). These data suggested that SHIV-infected neonate RMs had a less immunosuppressive GC environment associated with preferential induction of heterologous tier 2 HIV-1 NAb. In one adult dam BD62, we observed low Treg and high TFH levels (Fig. 5D, F), as well as a low ratio of TFR:TFH (Fig. 5H) that was associated with induction of heterologous HIV-1 NAb in this animal (Fig. 3B), similar to the neonate RMs that generated heterologous HIV-1 NAb. Moreover, Dam BD62 and neonates that generated heterologous HIV-1 NAb had high viral loads, thus supporting the notion that high viral load was associated with heterologous HIV-1 NAb induction.

To further interrogate the immunological environment in macaque LNs that was elicited by neonatal and adult SHIV-infection, we performed bulk RNA-seq on leftover LN cells from the phenotyping assays. For one young RM (V059), there were no leftover cells, thus we studied only 9 SHIV-infected RMs in bulk RNA-seq; 5 adult and 4 young RMs. We found that FOXP3 gene, a hallmark of Treg cells<sup>53,54</sup>, was significantly upregulated in SHIV-infected adult RMs compared to neonatal SHIV-infected RMs (Fig. 6A), suggestive of an increased immunosuppressive capacity of Tregs<sup>55</sup> in adult RMs. These data also aligned with our previous observation that adult SHIV-infected RMs had higher levels of Treg cells, as determined by flow cytometry (Fig. 5D). Compared to neonates, adult SHIV-infected RMs showed significant upregulation of genes crucial to the development and functions of FOXP3+ Treg cells compared to neonates (Fig. 6B), including *FOXP3*, *IL2* and *IL2 receptor (R)*<sup>56</sup>, *IL7R*<sup>57</sup>, and *CCR4*<sup>58,59</sup>. Moreover, gene set enrichment analysis (GSEA) of the DEGs between neonate and adult SHIV-infected RMs revealed multiple candidate pathways that may contribute to the immunologic milieu in the LNs of neonate compared to adult SHIV-infected RMs (Fig. 6C). Genes associated with pathways suggestive of Treg development controlled by FOXP3 were downregulated in neonate compared to adult SHIV-infected RMs, including *FOXP3*, *IL2* and *IL2RA* (Fig. 6). Genes linked to cytokine and cytokine receptor interactions were in the pathway that was most significantly downregulated in neonate SHIV-infected RMs compared to adults, and this pathway included genes associated with cytokine signaling in immunity that were also downregulated in neonate SHIV-infected RMs compared to adults (Fig. 6C). CCL22 has been shown to be generated by dendritic cells (DCs) in LNs and mediates binding to CCR4 on Tregs to promote Treg function<sup>58</sup>, consistent with significantly higher levels of CCL22 and CCR4 expression in adult SHIV-infected RMs (Fig. 6B), and an enrichment of genes associated with a pathway for dendritic cell response to HIV-1, in adult SHIV-infected RMs (Fig. 6C). Compared to adults, neonate SHIV-infected RMs had an enrichment of genes associated with transcription of HIV genome, HIV life cycle and HIV infection (Fig. 6C), consistent with higher plasma viral load in these animals (Fig. 1C). These data suggested that immunoregulation in the LN of SHIV-infected RMs contributes to neonatal immunity to HIV-1 that is associated with preferential heterologous HIV-1 NAb induction compared to adults.

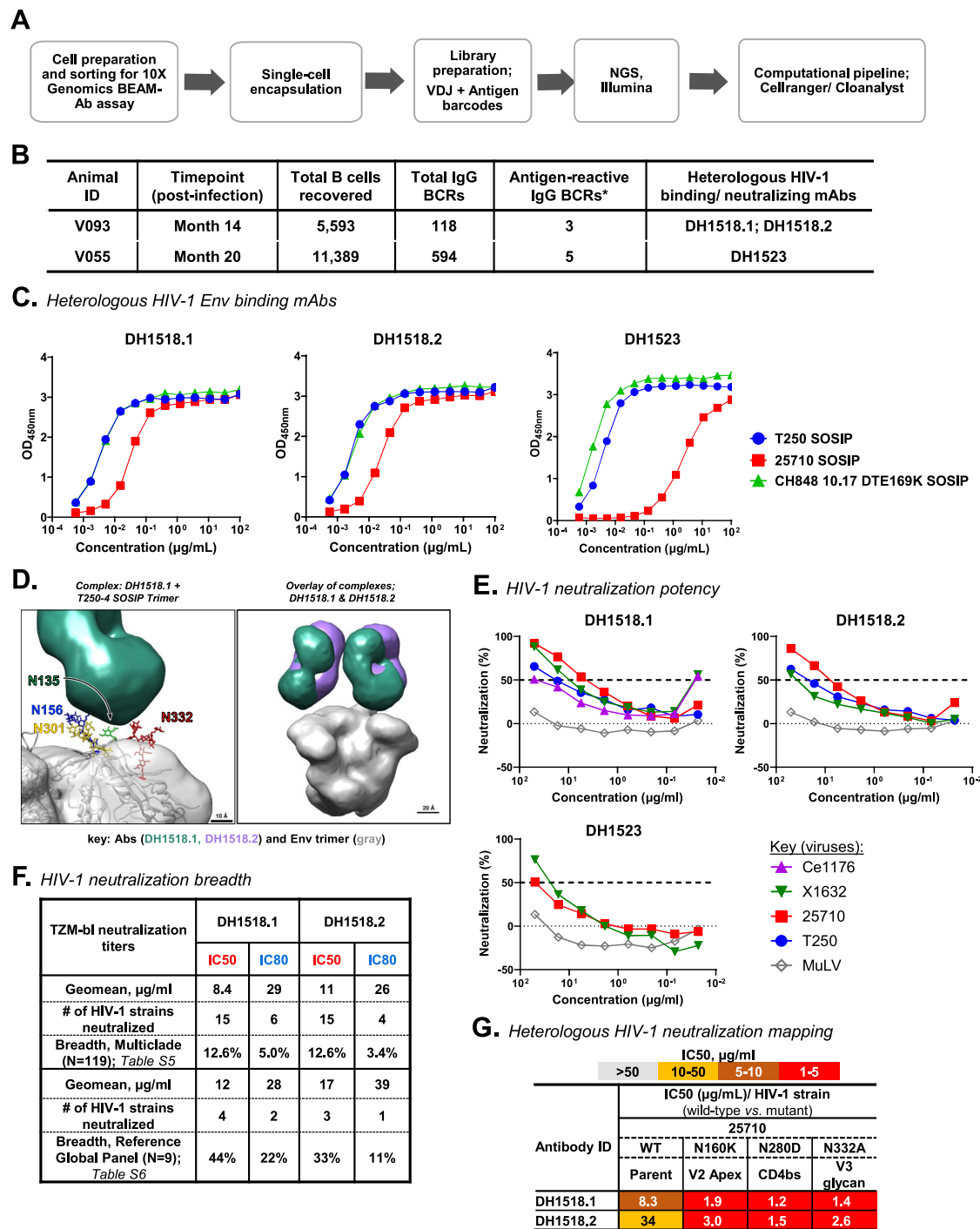
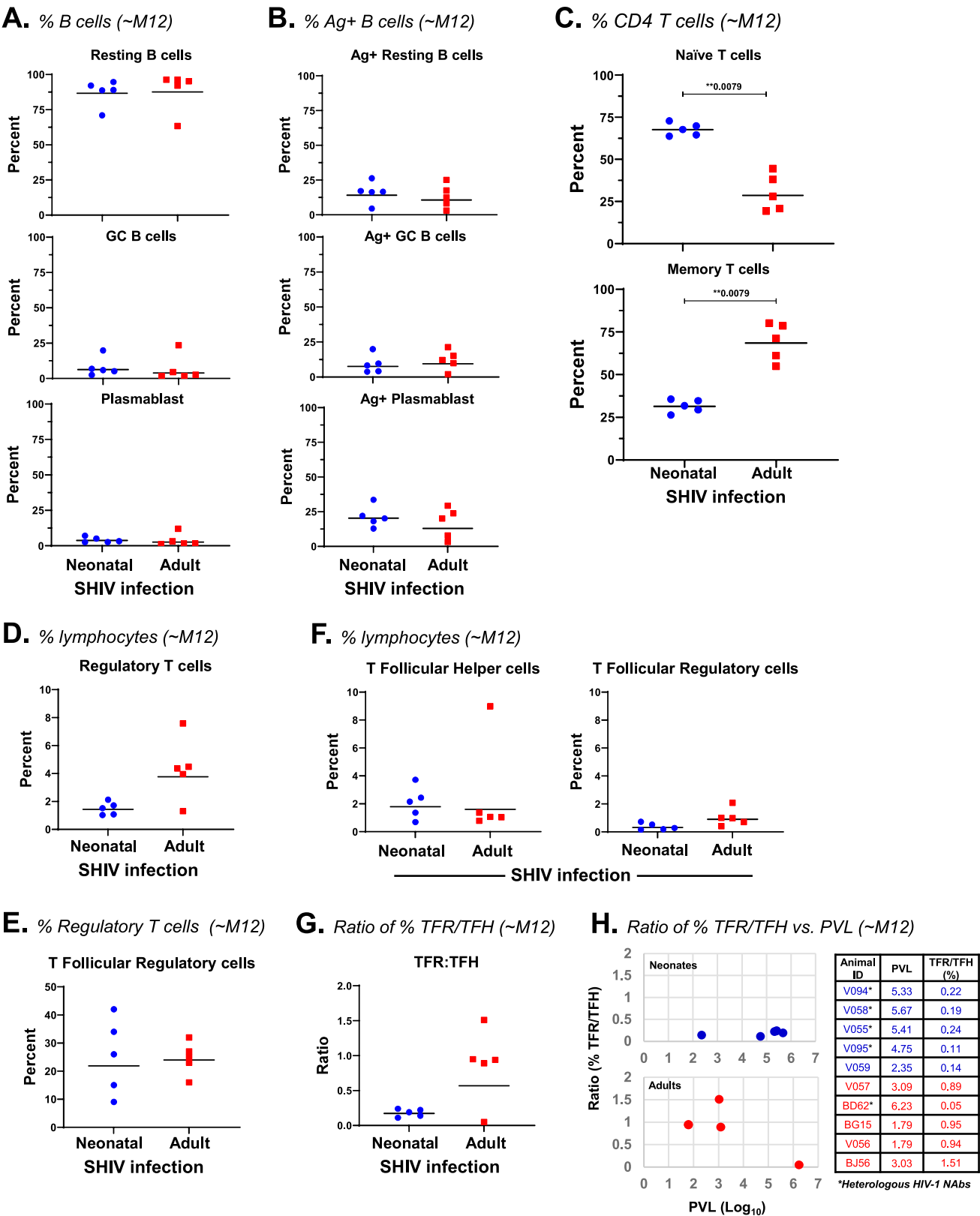


**Fig. 4 | Isolation and characterization of heterologous HIV-1 neutralizing mAbs in neonatal SHIV infection.** **A** Overview of BEAM-Ab (10X Genomics) pipeline and analytical plan used to isolate antigen-reactive B cells from representative RMs that generated plasma heterologous HIV-1 nAbs following neonatal SHIV infection. **B** Summary of BEAM-Ab assay outcomes from two representative RMs, V093 and V055, from which we isolated heterologous HIV-1 Env binding and nAbs; DH1518.1, DH1518.2 and DH1523. **C** Binding profile of DH1518.1, DH1518.2, and DH1523. MAb binding was measured via ELISA at OD<sub>450nm</sub> against heterologous and autologous SOSIP trimers used as B cell baits in BEAM-Ab. **D** (Left) NSEM structure of DH1518.1 (green) in complex with T250SOSIP trimer (gray). Candidate glycans within the mAb binding site are shown in different colors and labeled on the trimer. (Right) Overlay of DH1518.1 (green) and DH1518.2 (purple) in complex with the same T250 trimer. NSEM was performed with IgGs. **E** Neutralization curves of DH1518.1, DH1518.2, and DH1523 breadth with maximal neutralization titers against sensitive

heterologous tier 2 HIV-1 strains and MuLV. The percent viral quasi-species neutralized per virus at different mAb concentration is shown and the dash lines indicate 0 and 50% neutralization points; the latter may be used to determine IC<sub>50</sub> titer that achieves optimal neutralization. **F** Summary of neutralization titer and breadth of DH1518.1 and DH1518.2 against a panel of 119 heterologous tier 2 HIV-1 strains as well as the reference HIV-1 neutralization global panel of 9 heterologous strains; both panels were tested in separate laboratories. **G** Neutralization epitope mapping for DH1518.1 and DH1518.2 against HIV-1 25710, a representative sensitive heterologous tier 2 HIV-1 strain shown in panel (E). MAbs were tested for neutralization of HIV-1 bearing wild-type or mutant Env. Mutations were created to disrupt V2-apex (N160K), V3-glycan (N332A) and CD4bs (N280D) bnAb epitopes. Neutralization assays were performed in TZM-bl cells and titers reported as IC<sub>50</sub> in μg/ml as shown in the neutralization key. **B, C, E, G** Source data are provided as a Source Data file.



**Repertoire of immunoglobulin (Ig) genes from peripheral blood B cells**

In order to determine whether differences in the Ig gene repertoires between young and adult RMs also contributed to the development of heterologous tier 2 HIV-1 NAb, we next investigated the Ig gene repertoires in two neonate and adult-dam RM pairs where in one pair (Neonate - V093; Dam - V060) both neonate and dam generated

heterologous tier 2 HIV-1 NAb, whereas in the second pair (Neonate - V055; Dam - BG15) only neonate V055 generated heterologous tier 2 HIV-1 plasma NAb. We performed Illumina next generation sequencing (NGS) on Ig heavy and light chain genes from B cells in PBMCs from ~month 12 post neonatal and adult SHIV infection (Figs. 7, S8–S11).

Recombination of the variable (V), diversity (D) and joining (J) segments of the Ig heavy chain gene, and the V and J segments of the



**Fig. 5 | Germinal center dynamics of immune cell subsets in neonatal and adult SHIV infection.** Flow cytometry phenotype of immune cell subsets in LNs at ~12 months post neonatal and adult SHIV infection of RMs. All samples were collected from 12 months post-SHIV infection, except one dam who had samples collected at month 10 post-SHIV infection (see methods). **A** CD20+ B cells were further classified based on differential levels of Ki-67 and Bcl-6; resting B cells (Ki-67<sup>-</sup>, Bcl-6<sup>-</sup>), germinal center (GC) B cells (Ki-67<sup>+</sup>, Bcl-6<sup>+</sup>), and plasmablasts (Ki-67<sup>+</sup>, Bcl-6<sup>-</sup>). Resting, GC and plasmablast B cell subsets were reported as a percentage (%) of total LN B cells. **B** Autologous HIV-1 Env SOSIP trimer was used as a B cell bait to determine the percent of Ag-reactive B cells within each B cell subset. Antigen-reactive (Ag<sup>+</sup>) resting, GC and plasmablast cells were reported as a percent of total Ag<sup>+</sup> LN B cells. **C** Helper T cells (CD3<sup>+</sup>, CD4<sup>+</sup>) were further subdivided into naïve or memory subsets based on CD45RA levels (naïve, CD45RA<sup>+</sup>; memory, CD45RA<sup>-</sup>). These T cell subsets were reported as a percent of LN CD4<sup>+</sup> T cells. **D** Frequency of FOXP3<sup>+</sup> Tregs within the memory helper T cell subset. Tregs were

reported as a percent of total lymphocytes. **E** Frequency of TFR among Tregs. TFR cells were defined as CXCR5<sup>+</sup> and ICOS<sup>+</sup> among the FOXP3<sup>+</sup> Tregs. TFR cells were reported as a percent of Tregs. **F** TFH cells (PD-1hi, ICOS<sup>+</sup>) among the memory helper T cells, and TFR cells, shown as a percent of total lymphocytes. **G** Ratio of percent TFR to percent TFH within total lymphocytes in the LN. **H** (Left) Graph of ratio of % TFR:TFH and plasma viral load (PVL) in neonates and adults following ~12 months of SHIV infection; and (right) animal IDs with corresponding values for ratio of % TFR:TFH and PVL shown on the left. **A–G** These data were generated from a single experiment comparing cell subsets in neonate (*N* = 5) and adult (*N* = 5) RMs, and all graphs were generated in GraphPad Prism (v9 or v10) and statistics performed using two-sided Mann–Whitney testing; only statistically significant differences are indicated (*p*-values < 0.05). Geometric mean (horizontal bars) used for all comparisons except Ag<sup>+</sup> graphs where arithmetic mean was used to allow values of zero. **A–F** Gating hierarchy of immune cell subsets is provided in source data; Source data are provided as a Source Data file.

light chain genes, contribute to the antigen-binding domain and BCR diversity<sup>60,61</sup>. We found that all RMs used predominant variable heavy chain (VH) gene families 1 (VH1), 3 (VH3) and 4 (VH4) at a similar frequency (Fig. 7A) as described<sup>62,63</sup>, but they used varied frequencies of V-gene segments (Fig. S8A). For both heavy chain V- and D- segments, there were segments with similar frequencies across all animals as well as those with similar frequencies specific to each neonate and dam pair or each animal (Fig. S8A, B). All RMs used the same J-segments at similar frequencies (Fig. S8C). All four RMs studied had median HCDR3 length comprised of 13–14 amino acids (aa), but neonate V055 appeared to have a higher frequency of VH genes with longer HCDR3 length  $\geq 17$  aa (Fig. 7B). We detected VH genes of IgA, IgD, IgM, and IgG isotypes in all four RMs (Figs. 7C and S9). VH genes of IgD and IgM isotypes were predominantly unmutated or the least mutated compared to VH genes of IgA and IgG isotypes (Fig. 7C), in agreement with IgD and IgM B cells constituting the naïve B cell repertoire and IgA and IgG constituting the antigen-reactive B cell repertoires. Moreover, adult RMs had the highest mutated VH genes of all isotypes in agreement with more antigenic exposure with age. IgG was the most frequent isotype used by VH genes in all RMs (neonate, V055; neonate, V093; and adult, V060) that generated heterologous tier 2 HIV-1 NABs, in contrast with adult BG15 that generated only autologous tier 2 HIV-1 NABs and had more IgM than IgG (Fig. S9). Variations in the kappa (Fig. S10) and lambda (Fig. S11) light chain gene segments across animals remain to be fully explored for their roles in shaping the antibody repertoires in neonatal and adult SHIV infection. However, chi-squared statistical analysis of the Ig gene segment distributions in the VH or VL genes, and Kolmogorov–Smirnov (KS) test analysis of the mutation frequencies in Ig genes and HCDR3 length distributions, revealed that repertoire differences may not be driven by only relatedness of neonate and adult pairings or age of the animals (Table S6).

Heterologous HIV-1 NABs, DH1518, used IGHV4-NL17, IGHD3-41 and IGHJ5-4 gene segments, which were present in all animals, albeit at varied frequencies (Fig. S8A). These data suggested that the four RMs studied had the capacity of the Ig repertoires to support the generation of DH1518-like antibodies. Furthermore, we identified clonally-related DH1518 and DH1523 VH genes in the Illumina NGS datasets of VH genes from V093 and V055, respectively (Fig. S8A). These data suggested that DH1518 and DH1523 lineages started at or before month 12 post-infection.

### Env mutation patterns associated with the development of heterologous HIV-1 neutralization breadth

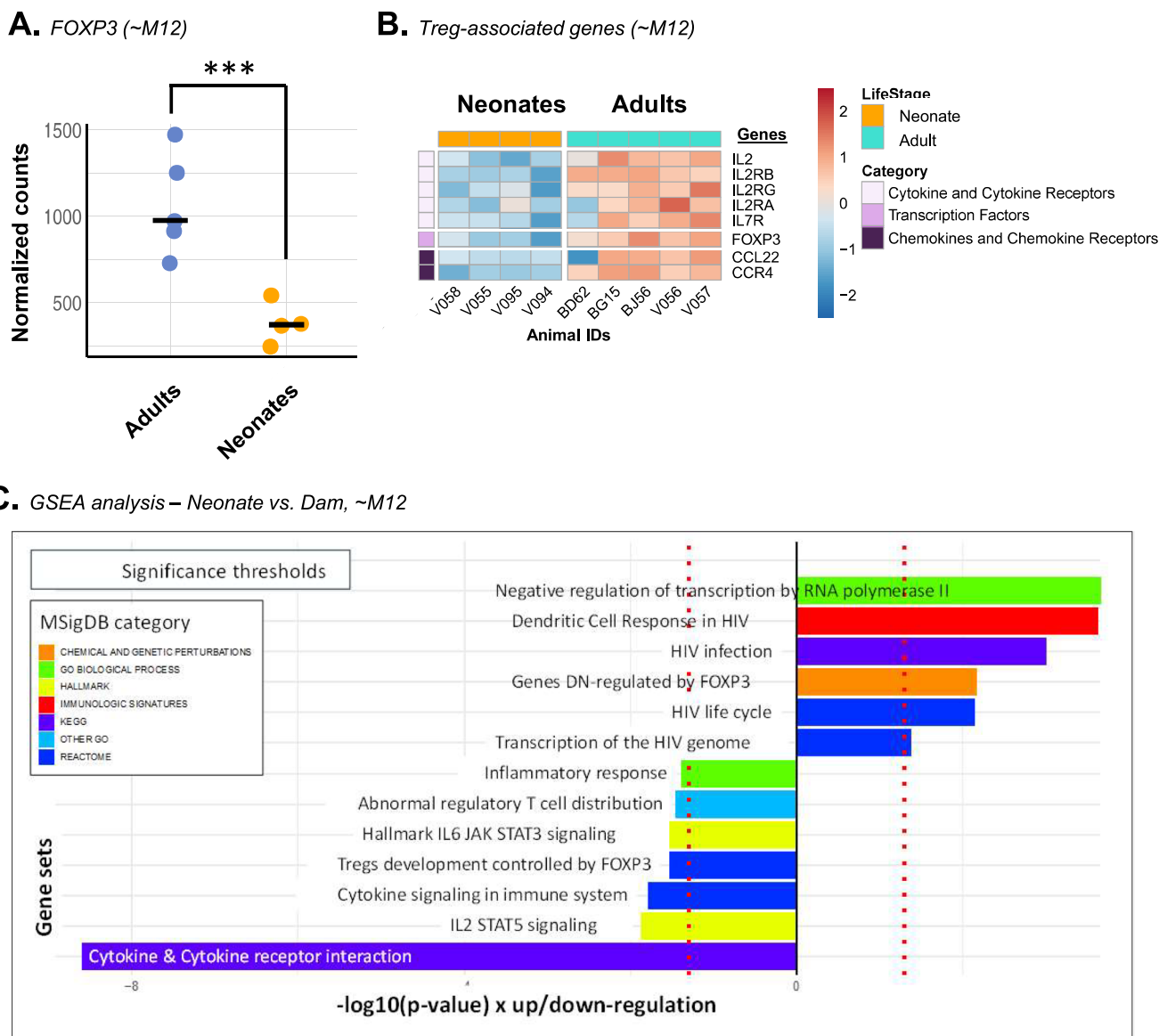
To identify *env* mutation patterns associated with HIV-1 neutralization breadth following SHIV-infection in neonatal and adult RMs, we performed sequence analysis on a total of 1,210 Envs from 12 neonate SHIV-infected RMs and 330 Envs from 5 adult SHIV-infected RMs (Fig. S12A). The 12 young RMs were previously described<sup>29</sup> and includes

11 RMs that were included in the current study due to the availability of the corresponding dam for comparison. For this analysis, we defined HIV-1 neutralization breadth as plasma (month 18) neutralization of  $\geq 30\%$  of heterologous HIV-1 strains in the virus panel that includes the global HIV-1 reference strains as described<sup>29,40</sup>; low-to-moderate HIV-1 neutralization breadth.

Using this definition of breadth, four of 12 SHIV-infected neonate RMs V058, V055, V093 and V331, developed breadth at the month 18 time point (Fig. 8A). We then performed a signature analysis for heterologous HIV-1 neutralization breadth; of all variable sites identified using the “Longitudinal Antigenic Sequences and Sites from Intra-Host Evolution” (LASSIE) algorithm<sup>28,64</sup>, the two most shared across animals were PNGS at HXB2 positions 133 and 138, which had been knocked out of the CH848 10.17 DT.E169K Env in the autologous SHIV but were completely restored in all RMs by month 6 (Fig. 8B). For all other sites identified by LASSIE, we used a Fisher’s Exact Test to identify those enriched in the group that developed HIV-1 neutralization breadth. The strongest association was with site 432 (*p*-value = 0.002) (Fig. 8B, C): at month 18, all eight neonate SHIV-infected RMs that did not develop HIV-1 neutralization breadth maintained the arginine (R) residue in the autologous virus whereas most sequences in the four RMs (V055, V058, V093 and V331) that developed breadth had a mutation to a lysine (K). By month 24, two RMs, V055 and V058, had no sequences still carrying the R residue. Position 432 is a CD4BS bnAb contact site and Bricault et al. found amino acid R to be associated with increased sensitivity to VRC07 CD4BS bnAb<sup>65</sup>.

Additionally, Env position 153 in V1 was significantly associated with HIV-1 neutralization breadth (*p*-value = 0.02), whereas sites 362, 139 and 327 were marginally associated (*p*-values = 0.06, 0.08 and 0.08, respectively) (Fig. 8B, C). Env positions 139 and 153 in V1 are proximal to sites 137 and 156 that houses V3 bnAb escape mutations and were found to be mutating in other SHIV-infected adult RMs<sup>28</sup>. Position 327 is part of the GDIR motif in the V3-glycan bnAb epitope at positions 324–327<sup>66,67</sup>, but in the CH848 10.17 DT.E169K SHIV challenge the motif encodes lysine at position 327 (K327). All 4 RMs that developed HIV-1 neutralization breadth completely reverted to R327 by month 6, whereas 5/8 (63%) RMs that did not develop breadth still retained the 327K residue in some of their sequences by the last sampled time point (Fig. 8B, C). A PNGS at position N362 is associated with V3 bnAb sensitivity<sup>65</sup> and by month 18, 3/4 (75%) RMs that developed HIV-1 neutralization breadth had almost completely lost the glycosylation site at this position, and in the fourth animal, V331, 30% of the sequences had lost it. On the other hand, of all the eight animals that did not develop HIV-1 neutralization breadth, only V095 showed a 60% drop in frequency of the PNGS at month 18, whereas all others either completely retained the glycan site or showed a < 10% decrease in frequency (Fig. 8B, C).

Next, to investigate whether the identified signature sites associated with heterologous HIV-1 neutralization breadth in neonatal SHIV

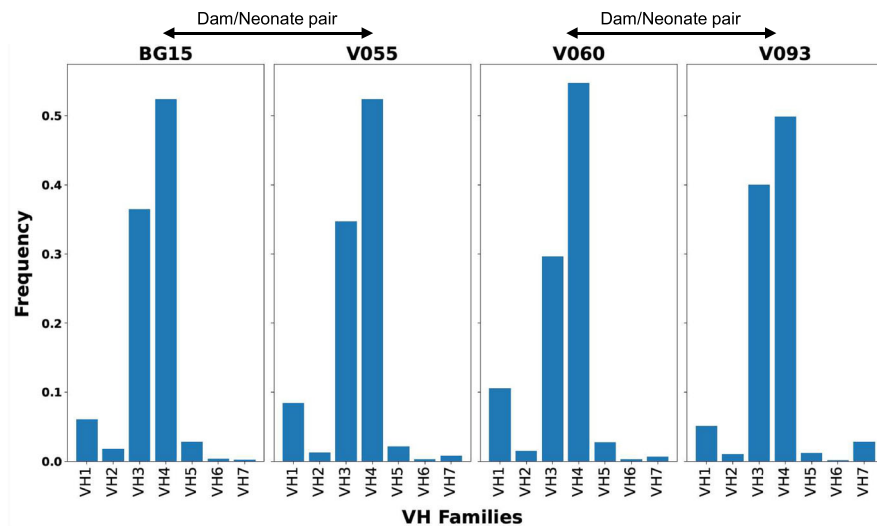
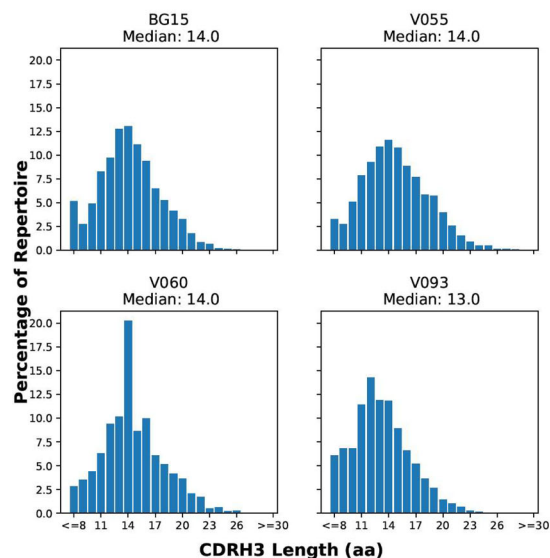
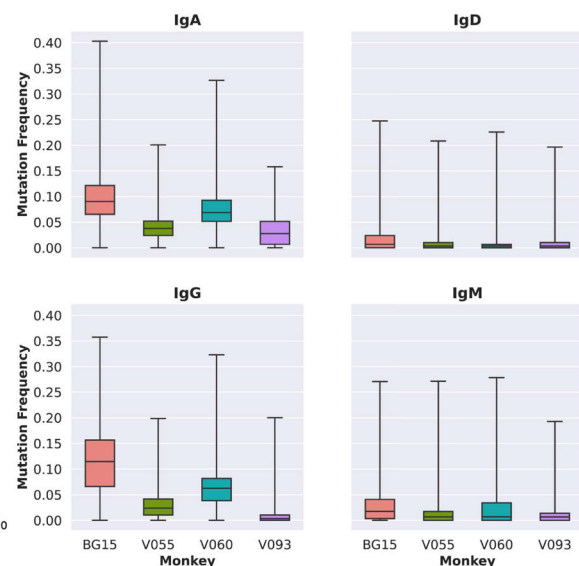


**Fig. 6 | Gene expression analysis of total lymph node (LN) cells following neonatal and adult SHIV infection.** Bulk RNA-seq analysis was performed on total LN immune cells ~12 months after neonate and adult SHIV infection. All samples were collected from month 12 post-SHIV infection, except one dam (V057) that had samples collected at month 10 post-SHIV infection. All 10 RMs studied generated autologous HIV-1 NABs, but 4/5 neonate (V055, V058, V094, and V095) and 1/5 adult (BD62) RMs generated heterologous tier 2 HIV-1 NABs. Genes were quality filtered, quantified and analyzed using various computational tools (see methods). **A** Gene expression levels of *FOXP3* in LNs of adult ( $N = 5$ ) and neonate ( $N = 4$ ) RMs using normalized count values by DESeq2; infants—242 (V094), 361 (V055), 383 (V095) and 541 (V058); adults—733 (BD62), 915 (BG15), 975 (V056), 1247 (V057) and 1477 (BJ56). Statistical analysis was performed using a two-sided Wald test for differential gene expression. The reported adjusted  $p$ -value of 0.0004 was obtained using the Benjamini-Hochberg procedure to control the false discovery rate (FDR), ensuring adjustments were made for multiple comparisons. **B** Expression levels of genes involved in the development and function of Treg cells, which were

significantly downregulated in neonates compared to adults around 12 months post-SHIV infection, as visualized in a heatmap. The key shows gene upregulation (red) versus downregulation (blue) in adult and neonate SHIV-infected RMs. **C** Gene set enrichment analysis (GSEA) performed using the *fgsea* R package with MSigDB's hallmark, curated, ontology, and immunologic signature gene sets to correlate gene expression changes in neonatal SHIV infection with relevant biological pathways. Directionality: gene sets enriched in upregulated genes shown on the right and those enriched in downregulated genes on the left. The enrichment score for each gene set is calculated using a weighted Kolmogorov-Smirnov statistic to measure the enrichment of each gene set using an ordered gene list.  $P$ -values are derived from 1000 permutations of gene labels, creating a null distribution of enrichment scores for comparison. The resulting  $p$ -values are adjusted using the Benjamini-Hochberg method to control the false discovery rate (FDR). This permutation method assesses the significance of the enrichment scores under the null hypothesis that gene labels are randomly associated with their expression changes (**A–C**) Source data are provided as a Source Data file.

infection were paired with the dams' ability to develop HIV-1 neutralization breadth, we looked at two specific neonate and dam pairs; one where the neonate (V058) developed HIV-1 neutralization breadth but the paired dam (BD62) did not, albeit meeting our criteria for heterologous HIV-1 NAB induction (Figs. 3B and 8D); and one pair of RMs where both animals developed HIV-1 neutralization breadth (V093/V060) (Figs. 3A, 8E). By month 18, neonate V058 was able to

neutralize 4/8 (50%) viruses (Fig. 8A), while the paired adult dam BD62 did not develop HIV-1 neutralization breadth (Fig. 3B). Logo plots at the five Env sites (139, 153, 327, 362 and 432) associated with HIV-1 neutralization breadth in neonatal SHIV infection showed that compared to the adult dam BD62, sequences from all paired neonate V058 carried K432 and G153 by month 18, whereas none of the sequences in BD62 carried G153 and only a minority fraction carried K432 (Fig. 8D).

**A.** *VH gene families***B.** *HCDR3 length distribution***C.** *SHMs in VH genes per isotype*

**Fig. 7 | Ig gene repertoires in neonatal and adult SHIV infection.** At month 12 post-infection, we interrogated the Ig gene usages and their immunogenetics that contribute to the B cell receptor (BCR) repertoires in neonate (V055 and V093) and adult (BG15 and V060) SHIV-infected RMs. Neonate and dam pairs: V055/BG15 and V093/V060. Shown are the frequencies of VH gene families VH1-VH7 (**A**), HCDR3 length distribution as percentages (**B**) and SHM frequencies of VH genes of different antibody isotypes (IgA, IgD, IgG and IgM) (**C**), used by BCRs of neonate and

adult SHIV-infected RMs. Frequencies were shown as a portion of 1 and percentages shown as a portion of 100. Macaque Ig genes were computationally inferred using macaque reference databases. For panel (**C**), the box is the interquartile range of 25th percentile to the 75th percentile of the data with the median also shown, and the whiskers show the upper and lower bounds of the mutation frequencies.

**A–C** Source data are provided as a Source Data file.

In the neonate and dam pair where both animals developed HIV-1 neutralization breadth, the adult dam V060 still carried less residues associated with breadth compared to the paired neonate V093 (Fig. 8E). However, contrary to BD62, some of the sequences in adult RM V060 carried residue 139E, and the frequency increased over time (from 21% at month 6 to 34% at month 16), whereas 139G, associated with lack of breadth, decreased from 52% at month 6 to 5% at month 16 (Fig. 8E). Furthermore, while the neonate V093 had completely lost the N362 glycan at month 18, in the paired adult V060 the glycan frequency was trending down at month 16 but was still 88% prevalent. While adult dam RMs showed distinct neutralization profiles and fewer breadth associated sites compared to their paired neonates, both dams by months 16–18 showed some evidence of increasing frequency in these sites (i.e. loss of the N362 glycan in both dams), consistent with

previous observations that neonate SHIV-infected RMs tended to develop broad responses earlier than adults.

Furthermore, to determine whether higher and earlier viral diversity in the neonate RMs influenced breadth development, we calculated the mean pairwise Hamming distances (defined as the number of mutations across every sequence pair) within each host as well as the mean Hamming distances from the challenge SHIV CH848 10.17 DT.E169K Env at every time point where sequence data was available. The four neonate SHIV-infected RMs that developed HIV-1 neutralization breadth (Fig. 8A) showed higher viral diversity slopes over time than the RMs that did not develop breadth and the paired adult-dams (Figs. S12B, D). Interestingly, at the first time point sequenced (month 4 for V249 and V252, month 6 for all other neonates), the mean Hamming distance was not significantly different



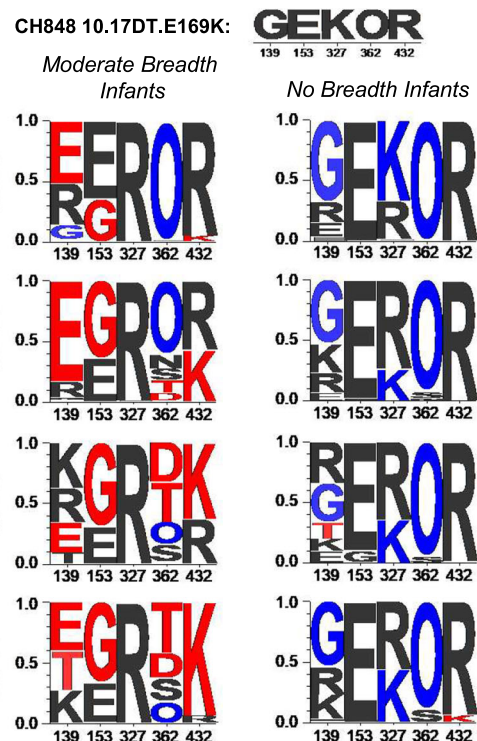
A

Heterologous HIV-1 neutralization breadth; Animal ID/ Frequency of HIV-1 neutralization (M18)											
V058	V055	V093	V331	V096	V252	V249	V095	V094	V253	V250	V059
4/8 (50%)	3/6 (50%)	4/9 (44%)	3/8 (38%)	1/6 (17%)	1/6 (17%)	1/7 (14%)	1/7 (14%)	0/6 (0%)	0/5 (0%)	0/5 (0%)	0/14 (0%)

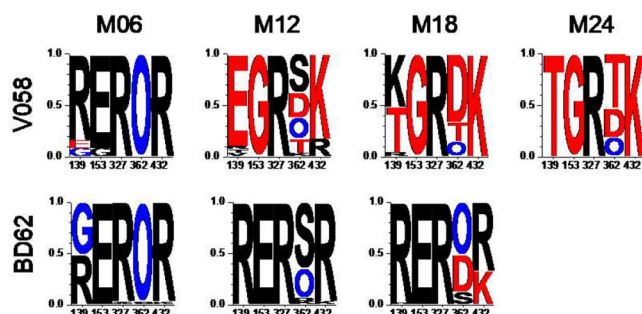
B

POS	N	V058	V055	V331	V093	V094	V095	V096	V249	V250	V252	V253	V059
133	12	V	V	V	V	V	V	V	V	V	V	V	V
138	12	V	V	V	V	V	V	V	V	V	V	V	V
269	11	V	V	V	V	V	V	V	V	V	V	V	V
347	11	V	V	V	V	V	V	V	V	V	V	V	V
289	10	V	V	V	V	V	V	V	V	V	V	V	V
344	10	V	V	V	V	V	V	V	V	V	V	V	V
336	10	V	V	V	V	V	V	V	V	V	V	V	V
230	8	V	V	V	V	V	V	V	V	V	V	V	V
327	7	V	V	V	V	V	V	V	V	V	V	V	V
139	7	V	V	V	V	V	V	V	V	V	V	V	V
169	7	V	V	V	V	V	V	V	V	V	V	V	V
400	6	V	V	V	V	V	V	V	V	V	V	V	V
137	5	V	V	V	V	V	V	V	V	V	V	V	V
429	5	V	V	V	V	V	V	V	V	V	V	V	V
268	5	V	V	V	V	V	V	V	V	V	V	V	V
231	5	V	V	V	V	V	V	V	V	V	V	V	V
461	5	V	V	V	V	V	V	V	V	V	V	V	V
59	5	V	V	V	V	V	V	V	V	V	V	V	V
340	5	V	V	V	V	V	V	V	V	V	V	V	V
397	5	V	V	V	V	V	V	V	V	V	V	V	V
432	4	V	V	V	V	V	V	V	V	V	V	V	V
640	4	V	V	V	V	V	V	V	V	V	V	V	V
178	4	V	V	V	V	V	V	V	V	V	V	V	V
339	4	V	V	V	V	V	V	V	V	V	V	V	V
362	4	V	V	V	V	V	V	V	V	V	V	V	V
396	4	V	V	V	V	V	V	V	V	V	V	V	V
464	4	V	V	V	V	V	V	V	V	V	V	V	V
399	4	V	V	V	V	V	V	V	V	V	V	V	V
291	4	V	V	V	V	V	V	V	V	V	V	V	V
407	3	V	V	V	V	V	V	V	V	V	V	V	V
136	3	V	V	V	V	V	V	V	V	V	V	V	V
187	3	V	V	V	V	V	V	V	V	V	V	V	V
209	3	V	V	V	V	V	V	V	V	V	V	V	V
348	3	V	V	V	V	V	V	V	V	V	V	V	V
607	3	V	V	V	V	V	V	V	V	V	V	V	V
153	3	V	V	V	V	V	V	V	V	V	V	V	V
155	3	V	V	V	V	V	V	V	V	V	V	V	V
409	3	V	V	V	V	V	V	V	V	V	V	V	V

C



D. Moderate Breadth by Neonate only



E. Moderate Breadth by Neonate and Dam

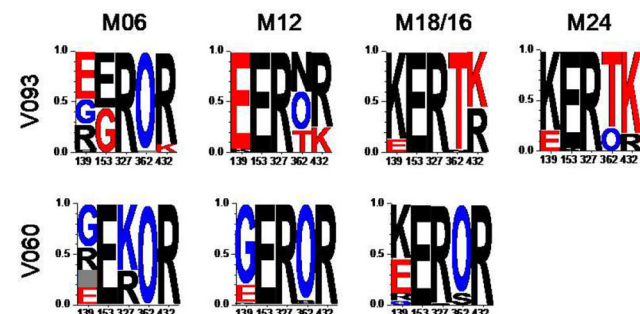


**Fig. 8 | HIV-1 Env Evolution Signature Analysis in Neonatal and Adult SHIV Infection.** **A** List of 12 total SHIV-infected neonate RMs that generated plasma heterologous HIV-1 NABs following SHIV CH848 10.17 DT.E169K infection as previously described<sup>29</sup>. Among the 12 RMs, eight had increasing plasma NAb titers against one or more heterologous HIV-1 strains as indicated. For the current study, we defined HIV-1 neutralization breadth (low-to-moderate) as neutralization of 30% or more viruses from the virus panel tested at month 18 (M18). Four RMs that developed HIV-1 neutralization breadth are indicated in red font. **B** LASSIE selected variability *env* sites that were shared across 3 or more animals (V = variable), ordered by most shared (top) to least. A site was defined to be variable if the LASSIE algorithm detected a loss of 50% or more of the corresponding CH8481017.DT.E169K residue at any given time point. Each column represents an animal, and animals that developed HIV-1 neutralization breadth are highlighted in yellow. Among all sites, 5 were significantly associated with breadth by Fisher exact test (shown in red box). **C** Logo plots at the 5 sites

significantly associated with HIV-1 neutralization breadth comparing animals that developed breadth (left) to those that did not (right). Residues of challenge virus CH8481017.DT.E169K at those positions are shown at the top. Residues more prevalent in one group but not the other are color coded; red, enriched in the breadth group; blue, the non-breadth group. **D**, **E** Logo plots at the 5 sites significantly associated with HIV-1 neutralization breadth comparing the neonate (top) to the paired dam (bottom). Residues are color coded red/blue according to whether they are found to be enriched in the HIV-1 neutralization breadth or non-breadth groups, respectively. In panel (**D**), we studied neonate V058 that developed breadth and by month 18 was able to neutralize 4/8 viruses, while the paired adult dam BD62 did not develop breadth (ID50 threshold of >60). In panel (**E**), we studied neonate V093 and paired adult dam V060 which both developed HIV-1 neutralization breadth by month 18 and 16, respectively, at the timepoints where we performed Env sequencing analysis. **C–E** Source data are provided as a Source Data file.



between RMs that developed HIV-1 neutralization breadth and those that did not, and the mean distance from the SHIV challenge Env was only marginally different ( $p$ -values = 0.4 and 0.04, respectively, by 1-sided Wilcoxon) (Figs. S12C, E). By month 18, when the four RMs developed HIV-1 neutralization breadth, both the mean Hamming distance and the mean distance from the SHIV challenge Env were statistically significantly different than all other 8 neonate RMs ( $p$  = 0.03 and 0.005, respectively by 1-sided Wilcoxon test) (Figs. S12C, E). These data suggested that higher and earlier viral diversity can potentially guide autologous antibodies toward broader heterologous responses.

### Association of virus load with heterologous HIV-1 neutralization activity in pairs of dam and neonate RMs

Since RMs that generated heterologous HIV-1 NABs seemed to have higher plasma viral load, we investigated the relationships between viral load and host immune responses. First, we used the area under the curve (AUC) of the log-transformed viral loads over time as a measure for comparison across animals and found that adult-dam RMs had statistically significantly lower AUC compared to neonates by 2-sided paired Wilcoxon test ( $p$  = 0.001) (Fig. S1, Table S7). Interestingly, all neonates with above-the-median AUC values, as well as the two adult-dams with the highest AUC among the adult RMs, developed heterologous HIV-1 NABs (Fig. 3, Table S7). Second, to test whether viral loads drove dam/neonate differences in autologous HIV-1 NAB responses developed by all the RMs (Fig. 2B, Table S2), we used random effect generalized linear model (GLM) regression using age group and viral load as independent variables. We confirmed statistically significant differences in viral loads between adults and neonates (Fig. 1C), but viral load was not a significant factor in any of the regression models including autologous HIV-1 neutralization titers. Third, we did observe a significant interaction between viral loads and age group when testing for differences in TFR to TFH ratios between the two populations, which was likely driven by dam BD62 (Fig. 5H), which developed heterologous responses and indeed had high viral loads at M18 and low TFR to TFH ratio. All other adult animals with lower viral loads had higher TFR to TFH ratio compared to neonates.

## Discussion

In the current study, we demonstrated that a higher frequency of neonate compared to adult RMs, infected with the same SHIV, generated heterologous HIV-1 NABs with characteristics of bnAbs, in agreement with previous reports that a higher frequency of infants and children LWH develop HIV-1 Env-reactive bnAbs<sup>7,17,18,68</sup>. Here, we also described heterologous HIV-1 NABs elicited by neonatal SHIV infection that potentially mapped to a unique discontinuous epitope on HIV-1 Env trimer, and defined Env evolution patterns associated with heterologous HIV-1 NAB induction in SHIV-infected neonate RMs that may be used to inform immunogen design in vaccine strategies to elicit these types of NAB responses, as described<sup>28</sup>. Moreover, phenotypic and RNA-seq expression studies of LN-derived cells in neonatal and adult SHIV infection implied that enhanced GC activity characterized by a less immunosuppressive environment constituted neonatal immunity associated with the induction of heterologous HIV-1 NABs that may be capable of developing into bnAbs. Overall, our data provide insights into the cellular and molecular mechanisms of pediatric immunity to HIV in a macaque SHIV infection model that may inform bnAb induction strategies in human infants and children.

SHIV-infected RMs developed plasma heterologous tier 2 HIV-1 NABs with limited neutralization breadth suggestive of bnAbs that have not yet fully matured. Young RMs following neonatal SHIV infection had neutralization titers of ~100–1000 ID50 that were as good or better than plasma NABs in HIV-1-infected human babies from whom a V3-glycan bnAb was isolated<sup>17,18</sup> and adult macaque SHIV infections from which bnAbs were isolated<sup>28,69</sup>, thus providing promise

for these SHIV infection models to interrogate the cellular and molecular mechanisms of bnAb induction. We used a high throughput antigen-specific strategy referred to as BEAM-Ab to isolate heterologous tier 2 HIV-1 NABs from two SHIV-infected neonate RMs, and found that two clonally-related NABs DH1518.1 and DH1518.2 targeted an epitope partially occluded by glycans. Both mAbs neutralized heterologous tier 2 HIV-1 strains, but had increased neutralization titers when a glycan is removed from V2-apex (N160) and V3-glycan (N332) bnAb epitopes. Epitope mapping of DH1518 mAbs in complex with HIV-1 Env trimers via NSEM was inconclusive, but raised the hypothesis that DH1518 mAbs may target discontinuous epitopes than span canonical bnAb-epitopes on two protomers of the trimer or an extended and flexible epitope; both of which have never been described for heterologous tier 2 HIV-1 Env-reactive NABs. Future studies will use high resolution structural analyses to conclusively map DH1518 epitopes on Env.

Immunoregulation in LN-derived GCs in representative RMs constituted a less immunosuppressive GC environment in neonatal SHIV infection that may be more permissive for bnAb induction as previously described in human HIV-infection<sup>21,46</sup>. Thome and colleagues reported that pediatric tissues had a higher proportion of Tregs (30–40%) among CD4<sup>+</sup>T cells compared to adults (1–10%), and pediatric Tregs express higher levels of FOXP3 compared to Tregs in adult lymphoid tissues<sup>3</sup>. These data support an increased suppressive capacity of Tregs in pediatric individuals to suppress endogenous T cell activation in an immature immune system<sup>3</sup>. That we observed lower Tregs in LN of neonatal SHIV-infected RMs compared to adults raised the hypothesis that elevated Tregs potentially linked with immunosuppression of GC activity during heterologous HIV-1 NAB induction is a feature of adult immunity that may contribute to a less permissive immunological environment for bnAb development. In this study, we evaluated a single timepoint post-infection for neonatal RMs, but future studies with longitudinal LN samples will fully define the dynamics of immunoregulation in the GCs associated with heterologous HIV-1 NAB induction in neonatal and adult SHIV infection.

We performed high-throughput genomics studies to gain insights into the Ig gene repertoires that may shape antibody responses in neonates and adult RMs. Ig gene segment rearrangements that contribute to the antigen-binding domain and BCR diversity is well known as a random process<sup>60,61</sup>, consistent with our findings of VH4\_NL17 gene segment usage among all four RMs studied but only V093 generated DH1518 heterologous HIV-1 NABs that used this gene segment. VH4\_NL17 appeared to be expressed at a higher frequency in V093 compared to the other three animals studied, thus suggesting an increased chance of making DH1518-like NABs. The more mutated IgG Abs were found in adult RMs V060 and BG15, suggestive of more B cells experiencing antigen-driven class switched recombination due to age and exposure to a myriad of antigens. Our study did not allow us to study only Ig gene repertoires in antigen-reactive B cells, but Roskin and colleagues demonstrated that PLWH who generated bnAbs had more mutated IgGs compared to PLWH who did not generate bnAbs<sup>44</sup>, thus suggesting a role for IgGs as bnAbs. However, mutated IgA antibodies have also been defined as bnAbs<sup>70</sup>, thus providing promise to further interrogate the mutated IgA B cell repertoire in V093, V055 and V060. Additionally, Illumina NGS of the Ig genes in RMs V093 and V055 revealed clonally-related VH genes of HIV-1 neutralizing B cell clones, DH1518 and DH1523, respectively, thus supporting the use of this technology in future studies to evaluate the maturation of DH1518 and DH1523 lineage antibodies over time as described<sup>69,71</sup>.

In human HIV-1<sup>37,72–74</sup> and RM SHIV<sup>28,29</sup> infection, candidate Envs were sought to guide vaccine induction of precursor bnAb B cell lineages through stages of affinity maturation to bnAb status<sup>15,43,75</sup>. Here, we report mutations and Env evolutionary features shared across neonatal SHIV-infected RMs that make heterologous tier 2 HIV-1 NABs. Some of these mutations emerged in bnAb epitopes<sup>65,66</sup>, suggestive of

antibody selection pressures as described<sup>28,29</sup>. Future studies will functionally evaluate the mutations in Envs that evolved over time with mutations suggestive of NAb pressure as described<sup>28</sup>. Our analysis of Env mutations was limited to samples with viremia  $\geq 10^3$  RNA copies/ml, but persistent high viremia was associated with the induction of heterologous HIV-1 NABs, suggestive of continual antigen selection of BCRs for affinity maturation and development of bnAbs<sup>29,31,32</sup>.

In conclusion, we demonstrated preferential development of heterologous HIV-1 NABs with characteristics of bnAbs in neonate versus adult RMs in a reproducible setting with the same virus; a study that cannot be done in humans. The results of our study provided insights into the mechanisms of neonatal immunity that contributes to a permissive environment for HIV-1 Env-reactive bnAb induction that may be harnessed by future pediatric vaccine strategies with appropriate immunogens and adjuvants to elicit heterologous HIV-1 NABs with bnAb characteristics in a permissive immunological environment. Neonates and corresponding adult-dams have shared genetic features that may shape host immunity in pediatric populations<sup>76</sup>. We showed that neonate and adult-dam RM pairs can have varying immune outcomes to the same SHIV, thus further studies with this type of unique model are warranted to fully investigate the impact of host genetics on specific immune responses to infection or vaccination against different pathogens.

Our study had limitations that should be considered when fully evaluating our results. First, due to the small sizes of neonate RMs, limited sample availability impacted the number of animals included in our serological and cellular assays. Second, our HIV-1 neutralization assays in TZM-bl cells used plasma and not purified IgG that may limit background interference with positive neutralization titers, thus we defined bnAb induction based on titers suggestive of affinity maturation. Moreover, we described plasma HIV-1 neutralization breadth as low-to-moderate given the criterion for a limited percentage of viruses neutralized in our Env signature analysis study. Third, bulk RNA-seq assay was performed on LN cells from a single timepoint of SHIV-infected adult and neonate RMs, and does not provide the capability for single cell analysis. Thus, we limited our analysis to whether we could find evidence of an immunosuppressive GC environment in adult RMs by studying known genes specific to certain immune cells observed in our phenotyping assays (for e.g. FOXP3 in Tregs). Fourth, we demonstrated the use of macaque Ig gene sequencing to identify potential differences in the Ig gene repertoires among neonate and dam pairs in the setting of SHIV infection, albeit a limited sample size. Improbable or rare mutations have been found to be associated with bnAb induction<sup>77</sup>, thus granular evaluation of Ig gene repertoires including potential improbable mutations will be needed to fully understand Ig gene repertoire differences that may impact heterologous HIV-1 NAB induction in neonatal versus adult SHIV-infected RMs. Fifth, our studies of heterologous HIV-1 neutralizing mAbs were limited to low antigen-reactive B cell recoveries via BEAM-Ab. Finally, despite differences in plasma viral load, neonates and adult RMs had some similar immune responses, but in our limited number of adult RMs with high viremia we found an association between viremia and induction of heterologous HIV-1 NAB induction as described<sup>29,32</sup>, suggestive of persistent antigen stimulation of B cell lineages for maturation to bnAb status<sup>43</sup>.

## Methods

### Experimental model

All Indian RMs (*Macaca mulatta*) were housed indoors at BIOQUAL, Inc., Rockville, MD, and were maintained in accordance with the Association for Assessment and Accreditation of Laboratory Animals with the approval of the IACUC. Research was conducted in compliance with the Animal Welfare Act and other federal statutes and regulations relating to animals and experiments involving animals and adheres to principles stated in the Guide for the Care and Use of

Laboratory Animals, NRC Publication, 2011 edition. All animal experiments performed in this study were approved by the Duke and BIOQUAL IACUCs. The term neonatal macaques was used to denote monkeys that were SHIV infected within early life as described in our study, while adults were listed as the dams that gave birth to the neonate monkeys. We studied six male and five female neonate RMs, and all 11 adult RMs were females. All RMs were tested for *Mamu*-alleles (A\*01, B\*08 and B\*017) found to be restrictive against SIVmac239 in RMs<sup>78–80</sup>. Based on genotyping for *Mamu*-alleles<sup>81</sup>, all 22 neonate and adult RMs were negative for *Mamu*-A\*01, but some of the neonate and adults were positive for *Mamu*-B\*08 or *Mamu*-B\*17.

All neonate RMs that were SHIV challenged were born via vaginal birth and dam-reared as performed in an independent study<sup>29</sup>. Animals ranged from day 4 – week 7 at the time of challenge that established infection. Sampling was limited in early life to prevent disruption of dam-rearing, thus not allowing for a robust evaluation of early life viral kinetics in all RMs. All dams were challenged with SHIV subsequent of dam-rearing to prevent SHIV antigen pre-exposure in the neonate RMs.

Animals were anesthetized as specified by the attending veterinarian during viral challenge. The administration sites (cephalic or saphenous), were shaved, prepped with isopropyl alcohol, and allowed to dry. A 1 ml TB syringe with 27-gauge needle pre-loaded with challenge virus (0.5 ml) was obtained. The vein was occluded by hand and the needle was inserted into vein. Placement of needle was confirmed by flash in the syringe and then inoculum was administered by slow bolus IV push. Needle was removed and firm pressure was placed on the site to prevent bleeding or hematoma formation. Animal was then returned to its housing unit.

### SHIV design and viral stock production

For construction and assessment for infectivity of SHIV CH848 10.17 N133DN138T (DT).E169K<sup>29,30</sup>, SHIV CH848 10.17 DT.E169K was generated in 293 T cells<sup>26,27</sup> and virus concentration was estimated by p27 antigen (p27Ag) ELISA (Zeptometrix). The SHIV bearing CH848 10.17DT.E169K Env was sensitive to neutralization by precursors and/or mature bnAbs targeting Env V2 and V3 regions, containing bnAb epitopes such as the V2-apex and GDIR-targeted V3-glycan sites<sup>29</sup>, thus making it a SHIV of interest for elicitation of multiple heterologous HIV-1 NABs in RMs.

### SHIV challenge in RMs

Twenty-one RMs were challenged with 5 or 50 ng p27Ag of SHIV CH848 10.17 DT.E169K inoculation intravenously (IV) in a final volume of 500 µl at BIOQUAL, Inc. using an established experimental approach<sup>29,30</sup>. One adult RM, V060, was challenged with 200 ng p27Ag SHIV CH848 10.17 DT.E169K in 1 mL of RPMI1640 with 10% FCS via IV inoculation followed by an additional intrarectal (IR) challenge of 200 ng SHIV. V060 failed to become infected after two challenges of 50 ng p27SHIV, hence the rationale for the combination challenge at a higher dose. All SHIV challenges were done at BIOQUAL, Inc. where the animals are housed and cared for. We established infection in one neonate with 5 ng p27 SHIV as initially planned; V094. However, some neonates were initially challenged with 5 ng p27 SHIV, but failed to establish infection, thus were subsequently re-challenged with 50 ng p27SHIV to achieve infection; V055, V058, V059, V093 and V095. Based on these initial observations, animals that were enrolled later in the study were challenged with only 50 ng p27 to establish infection; V096, V249, V250, V252, and V253. As for adults (dams), nine established infection from the initial challenge with 50 ng p27 SHIV; BG5, BD62, BJ56, V056, V061, V153, V151, V154 and V152. One adult RM V057 became infected only after a second IV challenge with 50 ng p27 SHIV, whereas another adult RM V060 only became infected after a third challenge with a higher dose of 400 ng total p27 SHIV (200 ng IV + 200 ng IR) as mentioned above. Interestingly, V060 is one of two adult RMs that generated heterologous HIV-1 NABs and while we did

determine whether the IV or IR challenge established infection, we (including this study)<sup>29</sup> and others<sup>26,27,31</sup> have shown that IV challenges can effectively establish infection following SHIV challenge.

In this study, none of the RMs were CD8-depleted prior to SHIV infection as described for other studies of bnAb induction following SHIV infection in adult RMs<sup>28</sup>. Here, we designed our studies to mimic natural HIV-1 infection in a SHIV macaque model where we could evaluate the capacity of the neonate versus adult immune systems in generating heterologous HIV-1 NABs with bnAb characteristics. However, we did not study mucosal viral transmission that would be mimicked via breastfeeding in neonatal RMs. Nelson et al.<sup>31</sup> studied oral SHIV infection of neonatal RMs and found that only a subset of those RMs generated autologous HIV-1 NABs during the short study duration of 12 weeks. It remains unknown whether oral SHIV infection that can mimic breastfeeding and the natural route of pediatric infection would elicit substantially different responses than those reported in this study.

Previous studies that have evaluated SIV and SHIVs in newborns and infant macaques demonstrated different outcomes than observed in this study in regards to viremia and disease progression<sup>82–84</sup>, suggestive of differences in the SHIV models that remain unknown. However, this is the first study to evaluate the induction and maturation of heterologous HIV-1 NABs in a rhesus infant SHIV infection model.

### Macaque blood processing

Anticoagulated RM blood was centrifuged and plasma was removed, aliquoted and stored at  $-80^{\circ}\text{C}$ , while PBMCs were separated from the remaining volume of plasma, buffy coat, and 5 mm of red blood cells as described<sup>29</sup>. PBMCs were washed and counted before being frozen down and then stored in liquid nitrogen. Coagulated RM blood was centrifuged and serum was removed, aliquoted, and stored at  $-80^{\circ}\text{C}$ .

### Macaque LN sampling and processing

Peripheral LNs were determined based on anatomy to locate inguinal LNs in the groin and axillary LNs in the arm pits, but LN sampling was performed via surgery by licensed veterinarians at BIOQUAL<sup>29</sup>. Additionally, LN processing was also performed for cryopreservation and storage in liquid nitrogen<sup>29</sup>. Briefly, the study animals were anesthetized with the appropriate anesthetic agents, as specified by the staff veterinarian. The area is first surgically prepared for biopsy and then the skin is sharply incised over or adjacent to the target LN site for isolation of the LN by blunt dissection. Peripheral LNs were determined based on anatomy to locate inguinal LNs in the groin and axillary LNs in the arm pits. Portions of isolated LNs were placed in tissue fixative or media prior to shipment overnight to Duke University accessioning unit for processing. For LN processing, sections of LNs were made in a petri dish containing RPMI + 10% FBS. Sections were then placed into Miltenyi gentleMACS C tubes and LN were dissociated using the Miltenyi gentleMACS OctoDissociator. Dissociated LNs were then passed through a 70  $\mu\text{m}$  cell strainer. Cells were washed. Following wash and counted before being frozen down and then stored in liquid nitrogen. All animals were studied using LNs collected at month 6 or 12 post-infection, except V057 that was behind on infection schedule and as such LN collection time points were months 5 and 10 post-SHIV infection. The LNs collected for neonatal RMs were primarily inguinal LNs<sup>29</sup>. LNs collected for the dams following SHIV infection were all inguinal LN for the first two collection timepoints within 12 months of infection, but later timepoints had a mix of inguinal and axillary LNs. Thus, we studied only inguinal LNs for immune cell phenotyping and bulk RNA-seq for neonate at month 12, and dams at months 5–6 and 10–12, post SHIV-infection.

### Viral load quantification

Viral load as RNA copies per milliliter of blood was quantified using a well-established laboratory developed two-step real-time qPCR

assay<sup>29</sup>. Here, a QIAAsymphony SP (Qiagen, Hilden, Germany) automated sample preparation platform along with a Virus/Pathogen DSP midi kit and the cellfree500 protocol was used to extract viral RNA from 500  $\mu\text{L}$  of rhesus plasma, and a reverse primer specific to the gag gene of SIVmac251 (5'-CAC TAG GTG TCT CTG CAC TAT CTG TTT TG -3') was annealed to the extracted RNA and then reverse transcribed into cDNA using SuperScriptTM III Reverse Transcriptase (Thermo Fisher Scientific, Waltham, MA) along with RNase Out (Thermo Fisher Scientific, Waltham, MA). The resulting cDNA was treated with RNase H (Thermo Fisher Scientific, Waltham, MA) and then added (2 replicates) to a custom 4x TaqMan™ Gene Expression Master Mix (Thermo Fisher Scientific, Waltham, MA) containing primers and a fluorescently labeled hydrolysis probe specific for the gag gene of SIVmac251 (forward primer 5'-GTC TGC GTC ATC TGG TGC ATT C -3', reverse primer 5'-CAC TAG GTG TCT CTG CAC TAT CTG TTT TG -3', probe 5'-/56-FAM/CTT CCT CAG TGT GTT TCA CTT TCT CTT CTG CG/3BHQ\_1/-3'). The qPCR was then carried out on a StepOnePlus™ or QuantStudio 3 Real-Time PCR System (Thermo Fisher Scientific, Waltham, MA) using the following thermal cycler parameters: heat to  $50^{\circ}\text{C}$ , hold for 2 min, heat to  $95^{\circ}\text{C}$ , hold for 10 min, then the following parameters are repeated for 50 cycles: heat to  $95^{\circ}\text{C}$ , hold for 15 s, cool to  $60^{\circ}\text{C}$  and hold for 1 min. Mean SIV gag RNA copies per reaction were interpolated using quantification cycle data and a serial dilution of a highly characterized custom RNA transcript containing a 730 bp sequence of the SIV gag gene. Mean RNA copies per milliliter were determined by applying the assay dilution factor ( $\text{DF} = 18.72$ ). SIV gag (SIV mac251) RNA copies were measured and reported as viral load. The limit of quantification (LOQ) for this assay was determined as approximately 62 RNA copies per milliliter ( $1.79\text{Log}$ ) of sample.

### Expression of mAbs

Recombinant mAbs were generated using commercially-obtained (GeneScript, Piscataway, NJ) plasmids with antibody heavy and light chain genes to transfect suspension Expi 293i cells using Expifectamine 293 transfection reagents (Thermo Fisher Scientific) via a well-established experimental strategy<sup>85,86</sup>. Purified recombinant mAbs were stored at  $-80^{\circ}\text{C}$ . All recombinant mAbs were expressed from plasmids encoding a macaque IgG constant region, and were QC'ed in western blot for appropriate heavy and light chain protein expression<sup>86</sup>.

### ELISA

Plasma and mAbs were tested for binding to synthetic peptides, and recombinant HIV-1 Env gp120 and stabilized chimeric SOSIP trimer in widely used ELISA<sup>29,69</sup>. Briefly, antigens were directly coated to Nunc-absorb (ThermoFisher) plates overnight at  $4^{\circ}\text{C}$  or captured using streptavidin, AbC- mAb (AVIDITY, Colorado, USA) mAb that were coated to Nunc-absorb plates overnight at  $4^{\circ}\text{C}$ . Unbound proteins were washed away and the plates were blocked with either goat serum-based (SuperBlock) or non-serum-based blocking media for 1 hour. Serial dilution of serum and mAbs were added to the plate for 60 min. Binding antibodies were detected with species-specific HRP-labeled anti-IgG Fc antibodies using 20  $\mu\text{L}$  per reaction with 1 h incubation at room temperature. HRP detection was subsequently quantified with 3,3',5,5'-tetramethylbenzidine (TMB). ELISA binding levels were measured at an optical density of 450 nm ( $\text{OD}_{450\text{nm}}$ ) and binding titers were analyzed as area-under-curve of the log-transformed concentrations ( $\text{Log AUC}$ ). Binding titers were graphically displayed using GraphPad Prism version 9 or 10.

Competitive ELISA was performed to assess cross-blocking of plasma and reference mAbs in a commonly used strategy<sup>29,37,87</sup>. Reference mAbs were biotinylated using the following product, Biotin-X-NHS, Cayman Chemicals, CAT# 13316, and tested for inhibition by competing non-biotinylated reference mAbs (PG9 and DH270) and plasma (1:50 dilution in triplicate wells). Binding inhibition was



measured as a percent of binding in the presence of competing Env V2 or V3 reactive mAbs, or plasma antibodies, relative to binding in the absence of a competing antibody. A successful assay had positive control blocking  $\geq 40\%$ .

### Antigen production for ELISA

The CH848 10.17 DT.E169K SOSIP trimer was produced in 293 F cells, purified with PGT145 affinity and gel filtration chromatography, and quality controlled for structural integrity via NSEM and binding profiles via Biolayer Interferometry (BLI); a well-established strategy for antigen production<sup>29</sup>. The CH848 10.17 DT.E169K gp120 monomer, V1V2 oligomers, and M.CON-S V3 peptide used in our studies were obtained from an inventory of these reagents for similar studies in the DHV1<sup>29,88–90</sup>. MN gp41 were commercially obtained (ImmunoDx, Woburn, MA, USA).

### Neutralization assays

Plasma and mAb neutralizing activities were assessed in TZM-bl cells; a commonly used experimental assay<sup>91</sup>. Plasma and mAbs were tested for neutralization against the global panel of HIV-1 reference strains, where a mixture of CH01 + CH31 bnAbs was used as a positive control for neutralization of all HIV-1 strains, and murine leukemia virus (MuLV) was used as negative retrovirus control<sup>40</sup>. For neutralization assays, a positive for neutralizing antibody activity in a sample is based on the criterion of  $>3\times$  the observed background against the MLV negative control pseudovirus. Neutralization potency or titer was reported as ID50 (reciprocal dilution).

Plasma from all RMs over time were tested for neutralization of CH848 10.17 E169K and CH848 10.17 DT.E169K SHIVs to demonstrate epitope mapping toward the V1 glycan hole (DT: N133DN138T) created by the design of the autologous SHIV CH848 10.17 DT.E169K<sup>29</sup>. For neonate RMs, we adapted a two-step approach to maximize the use of limited plasma volumes recovered from minimal blood draws to assess heterologous HIV-1 neutralization breadth<sup>29</sup>. First, plasma antibodies from all RMs at month 12–14 were tested for neutralization of all fourteen heterologous HIV-1 primary isolates at a higher final dilution ranging from 1:60–1:100. Second, these data were then used to identify viruses for each RM whose inflection on the neutralization curves were approaching or achieved 50% virus inhibition; these down-selected viruses were subsequently tested in neutralization assays against more concentrated longitudinal plasma per RM at the canonical 1:20 final dilution used in TZM-bl neutralization assays. For adult RMs, all plasma samples were tested at 1:20 final dilution. For this reason, the positivity cutoff values for HIV-1 neutralization and SVA-MLV negative control varies for samples across different timepoints for neonatal RMs (Table S2).

Our criteria for bnAb induction was described as having increasing titers of plasma NABs over time against  $\geq 1$  heterologous HIV-1 strain or persistent positive titers of similar magnitudes that were maintained over time against  $\geq 2$  HIV-1 strains<sup>29</sup>. We hypothesized that low level neutralization titers detected in some RMs that did not meet our criteria may be eliminated with purified IgG from the same plasma samples, but we did not perform IgG purification studies due to small blood draws because of the size of the neonate RMs and the potential of not recovering enough purified IgG for the extensive serology reported in this study. One young RM V253 had no indication of breadth at month 24, but at month 30 post infection has positive neutralization titers against additional viruses, suggestive of the development of breadth<sup>30</sup>. Thus, given the timeframe for this study of 24 months, we may be underestimating the frequency of neonatal SHIV-infected RMs that can generate bnAbs. On the other hand, none of the surviving dams had positive neutralization titers at month 24 (Table S2), but we cannot rule out that they may be slower to generate bnAbs and can do so at time points beyond 24 months of SHIV infection.

The viruses tested for neutralization in this study for plasma<sup>29</sup> and mAbs<sup>29,42,69</sup> included a multiclade panel of 119 heterologous tier 2 HIV-1 strains (Table S4)<sup>42,69</sup>, tested in the Seaman laboratory at Harvard, had some overlap with the smaller panel of 14 heterologous tier 2 viruses including the global panel viruses used to initially screen plasma and mAbs in the Montefiori lab<sup>29,40</sup>. We only observed discrepancies between the panels for T250-4 and Ce1176\_A3 where these viruses were weakly to moderately neutralized by DH1518 mAbs, but did not achieve IC50 when tested in the panel of 119 viruses. Neutralization breadth for mAbs were reported based on the results using the panel of 119 viruses as well as the global panel of 9 viruses (Fig. 4F), and highlights the need for standardization of virus panels to assess neutralization breadth of HIV-1 Env-reactive antibodies. Note that among the global panel of 9 viruses (Table S2), we studied BJOX010000.06.2, which is closely related to BJOX002000.03.2 that is referenced in the global panel<sup>40</sup>.

For neutralization mapping of mAbs, we used mutant Envs from 25710, X1632 and T250 HIV-1 strains that represented heterologous tier 2 HIV-1 strains neutralized by plasma from the SHIV-infected neonate RMs. The Env mutations include removal of glycans in bnAb epitopes, including N160K (V2-apex), N332A (V3-glycan) and N280D (CD4BS). However, HIV-1 25710 does not have a PNGS at Env position 280, thus enhanced neutralization due to N280D by DH1518 mAbs (Fig. 4G) may be facilitated by structural access to the bnAb epitopes targeted by these antibodies.

### Phenotyping of macaque LN cells

Cryopreserved LN biopsy cells were thawed and counted, and then resuspend at  $10 \times 10^6$  cells per mL of 1X PBS + 1%BSA;  $1 \times 10^6$  cells were aliquoted for each of the B and T cell assays, and the remaining cells were lysed in Qiagen buffer RLT for RNA extraction per manufacturer's protocol (Qiagen; Germantown, MD). All antibodies used for B and T cell phenotyping were titrated on rhesus PBMCs to ensure specificity and to determine optimal staining concentrations for flow cytometric sorting.

For **B cell staining**, a pretreatment with CD4 blocking antibody, Clone SK3 (Biolegend, San Diego, CA; Catalog #344602), was used to limit competition between the BCR and CD4 + T cells for binding the antigen in the BEAM Assemblies. After cell counting, LN cells ( $1 \times 10^6$ ) were resuspended into 100  $\mu$ L 1X PBS + 1%BSA + 5  $\mu$ M Chk II inhibitor, and 1  $\mu$ L anti-CD4 mAb per  $1 \times 10^6$  cells, for 10 min at room temperature. Surface and intracellular staining was conducted using the eBioscience™ FOXP3/Transcription Factor Staining Buffer Set (eBioscience, San Diego, CA; Catalog #00-5523-00). Surface cocktail of mAbs (Table S5) were added to cells and incubated for 20 min at 37 °C followed by washing via with 3 mL 1X PBS without BSA via centrifugation at 1500 rpm for 5 min. Only the B cell staining cocktail also included AF647-conjugated CH848.10.17 DT.E169K SOSIP to tag antigen-specific B cells. Cells were then resuspended with 500  $\mu$ L of viability dye in 1X PBS without BSA and incubated for 20 min at room temperature and protected from light. LIVE/DEAD™ Fixable Aqua was included for viability determination. Cells were then washed again with 2 mL 1X PBS/1%BSA at 1500 rpm for 5 min. We then followed the intracellular staining protocol summarized below.

For **T cell staining**, we followed the same procedures as outlined above on an additional  $1 \times 10^6$  LN cells with the exception of pretreatment with anti-CD4 mAb. Additionally, for the viability staining, cells were then resuspended with 500  $\mu$ L of viability dye in 1X PBS without BSA and secondary mAb PECy7-Streptavidin, and incubated for 20 min at room temperature and protected from light.

For the **intracellular staining** steps of both B and T cells, first we prepared 0.5 mL Fix/Perm buffer for each tube (includes compensation) and then incubated for 20 min at room temperature. Fix/Perm buffer is 1 part 4X Fix/Perm solution to 3 parts Fix/Perm diluent. Second, we prepared 1X Perm Buffer by diluting 10X perm buffer with deionized distilled water and then washed cells with 2 mL 1X Perm



Buffer at 1500 rpm for 5 min. Third, we washed cells for a second time with 1 mL 1X Perm Buffer at 1500 rpm for 5 min. Finally, intracellular staining solution was added to cells from second wash and incubated for 30 min at room temperature (see Table S5 for intracellular staining panel). Following the intracellular staining, cells were washed twice; (i) washed with 3 mL 1X Perm Buffer at 1,500 rpm/5 min; and (ii) washed with 2 mL 1X Perm Buffer at 1500 rpm/5 min. Cells were then resuspended in 300  $\mu$ L 1X PBS + 1%BSA and stored at 4 °C until data acquisition. Data were acquired via an LSRFortessa (DHV Flow Cytometry core) and analyzed using FlowJo (BD Biosciences).

### Macaque bulk RNA-seq of LN cells

We performed total RNA extraction using the RNeasy Plus Kits (Qiagen, Germantown, MD; Catalog #74134) on LN cells (range: 2.4–9.4 million cells per RM) from neonate and adult SHIV infected RMs. We obtained a range of 13.7 to 96.1 ng/ $\mu$ L total RNA in 50  $\mu$ L nuclease-free water. Up to 1000 ng total RNA per sample was used to generate sequence-ready libraries for Illumina NGS with the TruSeq RNA Sample Preparation Kit v2 (Illumina, San Diego, CA; Catalog #RS-122-2001). The quality of gene libraries for Illumina sequencing was assessed on a TapeStation 2200 with the high sensitivity D5000 ScreenTape (Agilent Technologies, Santa Clara, CA; Catalog #5067–5592), and their quantities were determined using the Qubit 3.0 fluorometer (Thermo Fisher, Waltham, MA; Catalog #Q33216). Gene libraries were sequenced using the NextSeq 2000 P3 200 cycles kit (Illumina; Catalog #20046812) to generate 2  $\times$  101 paired end reads following the manufacturer's protocol (Illumina, Document #200027171 v02) with loading concentration of libraries at 750 pM plus 1% PhiX (Illumina; Catalog #FC-110-3001) that allowed us to target up to 160 M million pair-end reads per sample.

### Bulk RNA-seq data analysis

Quality control of the RNA-seq samples was conducted using the FastQC tool [<https://www.bioinformatics.babraham.ac.uk/projects/fastqc/>]. Following this step, the Trim Galore toolkit [[https://www.bioinformatics.babraham.ac.uk/projects/trim\\_galore/](https://www.bioinformatics.babraham.ac.uk/projects/trim_galore/)], integrating Cutadapt<sup>92</sup>, was utilized to trim low-quality bases and eliminate Illumina sequencing adapters from the 3' ends of the reads. Alignment of the reads to the Mmul\_10 version of the RM genome and transcriptome<sup>93</sup> was achieved using the STAR RNA-seq alignment tool<sup>94</sup>. Only reads uniquely mapping to a single genomic location were considered. Gene expression was quantified using the HTSeq tool<sup>95</sup>. Only genes with at least 10 reads in any library were considered for further analysis. For normalization and differential expression analysis, the DESeq2<sup>96</sup> and Bioconductor<sup>97</sup> packages in the R statistical programming environment [<http://www.r-project.org>] were employed. The false discovery rate was computed to control for the risk of false positives arising from multiple hypothesis testing. Finally, gene set enrichment analysis<sup>98</sup> (GSEA) was performed utilizing MSigDB [<https://www.gsea-msigdb.org/gsea/msigdb/index.jsp>] gene sets from the hallmark, curated, ontology and immunologic signature collections. This analysis facilitated the correlation of observed gene expression changes with relevant biological pathways and signatures.

### NGS of macaque Ig genes

Ten million PBMCs at month 12 (BG15, V055, V093) or 13 (V060) post-SHIV infection from two neonate and dam pairs (BG15, dam/ V055, neonate; and V060, dam/ V093, neonate) were used to prepare NGS gene libraries using the customized SMART-Seq Human BCR (with UMIs) kit (Takara Bio, San Jose, CA; Catalog #634777) that replaced human BCR primers with proprietary Rhesus BCR primers (in pre-commercial status). This SMART-Seq kit fitted with rhesus primers was also used in a pilot experiment to amplify antibody heavy and light chain genes for a non-SHIV-infected RM, and these genes represented all macaque immunoglobulin genes in the KimDB reference database,

and all isotypes were represented as well. For this experiment with PBMCs from SHIV-infected RMs, total RNA was extracted from PBMCs using RNeasy Plus Kits (Qiagen, Catalog #74134) and RNA was eluted in 30  $\mu$ L nuclease-free water. We recovered RNA at concentrations ranging from 8.8–122.4 ng/ $\mu$ L. Up to 9.5  $\mu$ L total RNA was used for cDNA synthesis, BCR amplification, and generation of sequence-ready libraries following the manufacturer's protocol. The quality of BCR gene libraries for sequencing was assessed on a TapeStation 2200 with the high sensitivity D1000 ScreenTape (Agilent Technologies, Catalog #5067–5582), and their quantities were determined by Qubit 3.0 fluorometer (Thermo Fisher, Catalog #Q33216). Gene libraries were sequenced using the NextSeq 2000 P2 600 cycles kit (Illumina, Catalog #20075295) to generate 2  $\times$  301 paired end reads following the manufacturer's protocol (Illumina, Document #200027171 v02) with loading concentration of libraries at 750 pM plus 20% PhiX (Illumina, Catalog #FC-110-3001), thus allowing us to target at least 25 million pair-end reads for heavy chain, and at least 25 million pair-end reads for light chain per sample.

### NGS data analysis

Paired sequences were merged, and sequences with ninety-five percent of bases having a Q score  $\geq 30$  were retained. One sequence was randomly chosen for each UMI, and the sequences were then deduplicated after removal of the UMI and the 3' random 7-mer that is part of library construction. For the heavy chain library, gene segment annotation, HCDR3 identification, and V mutation frequencies were done with the Partis software package [<https://pubmed.ncbi.nlm.nih.gov/31329576/>] using the reference library from [<https://pubmed.ncbi.nlm.nih.gov/33484642/>] and custom scripts. Only sequences with in-frame rearrangements, non-mutated invariants, absence of frame shifting indels, and no stop codons were retained for further analysis. Isotype assignment was done with a custom script that used local alignment of the sequence 3' of the variable region sequence to a reference rhesus constant sequence database. Sequences were assigned to the isotype class of the reference sequence that returned the best hit, conditioning on the best hit being  $\geq 90\%$  of the best possible alignment score and the constant sequence query being longer than ten nucleotides. For the light chain library, sequences were classified into lambda, kappa, heavy, reverse complement, and other using a custom Convolutional Neural Network (CNN) that was trained on rhesus heavy, lambda, and kappa sequences where the length of constant regions approximate those in the Takara sequence ready gene library. Lambda and kappa sequences for further analysis were those that were classified as "Lambda" or "Kappa," respectively by the CNN with probability  $\geq 0.9$ . For the light chain gene libraries, gene segment annotation and V mutation frequencies were performed with the Cloanalyzer software package and custom scripts. All sequences where a rearrangement could be identified were used for downstream analysis.

### BEAM-Ab isolation of Env-reactive B cells

**Production of BEAM-Ab assemblies for B cell sorting.** To isolate antigen-reactive B cells, we first generated assemblies of antigens coupled to a BEAM Conjugate that contains 10X barcoded streptavidin molecule linked with a PE fluorescence marker. The BEAM Assemblies served as B cell baits or hooks for antigen-reactive B cells, and were generated according to the 10X Genomics Barcode Enabled Antigen Mapping (BEAM) Workbook for BEAM-Ab Assembly (Doc CG000597 Rev A). The biotinylated proteins used to make BEAM Conjugates were HIV-1 Env antigens (CH848 10.17 DT.E169K SOSIP, CH848 10.17 DT SOSIP, CH848 10.17 DT\_N332T SOSIP, T250 SOSIP, and 25710 SOSIP) and a non-relevant HIV antigen as Coronavirus N Protein N-Terminal Domain (NTD); these proteins were generated in the Saunders lab at DHV. One assembly contained no antigen and was prepared as a negative control (volume was compensated by 1X PBS) for background subtraction (see BEAM scoring).

All reagents were thawed on ice for BEAM Assembly production. Antigens were diluted in 1X PBS to a concentration of 0.5  $\mu\text{g}/\mu\text{L}$ , total volume of 100  $\mu\text{L}$ . The assemblies were produced with a scaling factor of 1 at 1,000,000 input cells per assembly. PBS was aliquotted for each assembly into amber eppendorf tubes to reach a final volume of 40  $\mu\text{L}$  after addition of BEAM Conjugate and antigen. Amber tubes from this point were kept on ice or at 4 °C on the Eppendorf ThermoMixer C. The antigen molecular weight (Da) and 10X Genomics recommended concentration (0.5  $\mu\text{g}/\mu\text{L}$ ) were entered into the 10X Genomics BEAM Workbook for BEAM-Ab Assembly on the tab for Step 2 of BEAM-Ab Assembly to obtain the volume of antigen necessary to produce the assemblies. To the PBS aliquots in each amber eppendorf tube, 2  $\mu\text{L}$  of respective BEAM Conjugate was added followed by the calculated amount of diluted antigen needed for a total of 40  $\mu\text{L}$  per assembly using the BEAM Workbook; this mixture was then mixed 10 times by pipetting. The amber tubes with the assemblies were then incubated in the dark at 4 °C on the Eppendorf ThermoMixer C for 30 min while shaking at a rate of 700 rpm. Assemblies were then transferred back on ice and 5  $\mu\text{L}$  of Quenching Reagent was added to each assembly on ice and mixed 10 times by pipetting. The quenched assemblies were then incubated again on the ThermoMixer for 30 min in the dark at 4 °C while shaking at a rate of 700 rpm. Afterwards, the assemblies were then centrifuged at 2500  $\times g$  for 5 min at 4 °C. Assemblies were stored at 4 °C to be used for cell staining in the sorting component of BEAM-Ab within 24 h of being produced or aliquotted as desired and stored at -80 °C for subsequent use.

**QC of BEAM assemblies.** We QC'ed BEAM Assemblies for binding to mAbs with known reactivities to the antigens in the assembly. Here, antibody-coated beads were used for the respective antigens on the assemblies in a flow-cytometry based assay. Each mixture of quenched assembly was diluted in 1X PBS to a final volume of 50  $\mu\text{L}$ ; for this calculation, the initial molar concentration of each assembly was set at 833 nM (guided by 10X Genomics Workbook) and post dilution concentration was set at 180 nM, thus we calculated the amounts of quenched assembly needed to achieve 180 nM in 50  $\mu\text{L}$ . Subsequently, the quenched assembly in 1X PBS was used to perform a 2-fold dilution three times in a 96-well plate for a total of 4 wells per assembly ranging in concentration from 180 nM to 22.5 nM (for a final volume of 50  $\mu\text{L}$ ). Separately, antibody-coated beads (Influenza HA-reactive, CH65 as a negative bead control; and positive control beads included HIV-1 Env targeted mAbs, CH01, PGT128, and 2G12, and NTD-reactive mAb, Ab026013) were pipette mixed and then diluted in 1X PBS in separate wells on the dilution 96-well plate. Each well needs 25  $\mu\text{L}$  per bead mixture; 24  $\mu\text{L}$  1X PBS + 1  $\mu\text{L}$  bead mixture (0.2  $\mu\text{L}$  positive beads + 0.8  $\mu\text{L}$  negative beads). On a filter-bottom 96-well plate (Millipore Sigma, Rockville, MD; Catalog #MABVN1250), 100  $\mu\text{L}$  of 1X PBS was added to each well to soak the filter, then aspirated using a vacuum manifold. Twenty-five microliters (25  $\mu\text{L}$ ) of the serially diluted assemblies were then added to the freshly aspirated filter plate in respective wells, followed by 25  $\mu\text{L}$  of the respective bead mixtures for a total of 50  $\mu\text{L}$  of beads and diluted assembly across 4 wells per assembly. One well per bead set was also designated as unstained and received 25  $\mu\text{L}$  of beads only. The filter plate was set to incubate in the dark at 4 °C on the ThermoMixer shaking at a rate of 700 rpm for 30 min then gently aspirated using the vacuum manifold. 100  $\mu\text{L}$  of 1X PBS was added to each reagent-containing well before being aspirated again. These washes were repeated for a total of three washes before re-suspending in 100  $\mu\text{L}$  of 1X PBS. The plate was then loaded onto the iQue3 Flow Cytometer and read using the PE channel. Data Analysis was performed using FlowJo 10 software. Following gating for singlets and using the unstained wells as a reference, the presence of two distinct populations, one of which was BEAM Assembly binding to positive control antibody-coated beads, was used as a qualitative measure of successful conjugation.

The antibody-coated beads were generated by activating Carboxyl Polystyrene Particles (SpheroTech, Lake Forest, IL; Catalog #CP-30-10) with N-Ethyl-N'-(3-dimethylaminopropyl) carbodiimide Hydrochloride (Millipore Sigma, Rockville, MD) and then incubating with antibody for two hours, followed by washes with 1X PBS + 1% BSA + 0.02% Sodium Azide.

**Cell staining and sorting.** Cryopreserved PBMCs were thawed at 37 °C and slowly diluted in 1 mL RPMI with 10% FBS (complete RPMI, cRPMI) plus Benzonase at 25 U/mL. After 1 min, the cell suspension was further diluted with 13 mL cRPMI. Cells were washed via centrifugation for 3 min at 400rcf, then resuspended in cRPMI at 2X10<sup>6</sup> cells/mL final concentration based on the frozen cell count. After cell resuspension, an aliquot (10  $\mu\text{L}$ ) was taken for cell count verification using the Cytex® Guava® Muse® Cell Analyzer (DHVI Flow Cytometry core). Following centrifugation, the cells were resuspended in 100  $\mu\text{L}$  of 1X PBS with 5  $\mu\text{M}$  Chk2 inhibitor (Millipore Sigma; Catalog #220486) and CD4 blocking antibody, Clone SK3 (Biolegend; Catalog #344602) at 1  $\mu\text{L}$  per 1X10<sup>6</sup> cells added to the final volume of 100  $\mu\text{L}$ ; keep the reaction on ice. An aliquot of 0.4–0.5  $\times 10^6$  cells was set aside as a negative control without BEAM antigens, but stained with the rest of the panel. The remaining cells were stained with surface antibodies for flow sorting (Table S5) and several BEAM Assemblies with PE fluorophore per experiment for 30 min on ice. Cells were stained with the antibody staining panel in 1X PBS + 1%BSA at a final concentration of 1X10<sup>6</sup> cells/100  $\mu\text{L}$ . Following cell staining, cells were washed with 1X PBS, then resuspended in 1 mL 1X PBS with 5  $\mu\text{M}$  Chk2 inhibitor + 1  $\mu\text{L}$  per 1X10<sup>6</sup> cells of Aqua vital dye for 30 min on ice in the dark. Cells were then washed with 1X PBS once followed by washing with 1X PBS + 1% BSA and, finally, resuspended in 100  $\mu\text{L}$  per 1X10<sup>6</sup> cells in 1X PBS + 1% BSA + 5  $\mu\text{M}$  Chk2 inhibitor and kept on ice. BEAM Assembly positive cells were sorted into 100  $\mu\text{L}$  1X PBS with 10% FBS or 500  $\mu\text{L}$  cRPMI in a 1.5 mL tube using a 100  $\mu\text{m}$  nozzle on a BD FACSymphony S6 (DHVI Flow Cytometry core). Sorted cells were kept on ice for no more than 1 h and then centrifuged at 400  $\times g$  for 3 min. The supernatant was slowly aspirated and discarded while leaving behind ~100–200  $\mu\text{L}$  of residual cells in buffer to target 400–2000 cells/ $\mu\text{L}$  as per 10X Genomics recommendations. The resuspended cells were then loaded into single cell GEMs using the Chromium Controller microfluidics chip and reverse transcription kit (10X Genomics).

For both V093 M14 and V055 M20, we used the following BEAM Assemblies: CH848 10.17 DT.E169K SOSIP, CH848 10.17 DT SOSIP, CH848 10.17 DT\_N332T SOSIP, T250 SOSIP, NTD and No-antigen. For V093 M14, we used an additional BEAM Assembly containing 25710 SOSIP.

**Gene library prep and sequencing.** We flow sorted 31,478 B cells from V093 (M14) and 83,010 cells from V055 (M20), quantified via the Countess 3, using the BEAM Assemblies described above. The sorted cells were used to generate VDJ, gene expression and BEAM barcode libraries, respectively, through Chromium Next GEM single Cell 5' Reagent Kits v2 (10X Genomics; Catalog #PN-1000263) with Feature Barcode technology for BEAM per the manufacturer's recommendations (10X Genomics, Document #CG000591 Rev A). One modification was the use of rhesus Ig constant region primers to generate the VDJ libraries that we established in an independent study<sup>69</sup>. For single cell encapsulation, we input all the cells recovered as quantified above into 2–5 lanes of the 10X Genomics CHIP, thus allowing us to target 20,000 cells for V093 (M14) and 50,000 cells for V055 (M20). After preparation of the gene libraries, we performed library QC was performed using TapeStation 2200 with the high sensitivity D1000 ScreenTape (Agilent Technologies, Catalog #5067–5582) and Qubit 3.0 fluorometer (Thermo Fisher Scientific, Catalog #Q33216). The qualified VDJ, gene expression and BEAM libraries were pooled at 1:10:1 ratio, and sequenced with NextSeq 2000 P3 100 cycles kit (Illumina, Catalog

#20074933) to achieve the sequencing depth of  $\geq 5,000$  read pairs/cell for VDJ libraries,  $\geq 50,000$  read pairs/cell for 5' gene expression libraries, and  $\geq 5000$  read pairs/cell for BEAM libraries following the manufacturer's protocol (Illumina, Document #200027171 v02). For Illumina NGS, we loaded concentration of libraries at 750 pM and 1% Phix (Illumina, Catalog #FC-110-3001).

**BEAM-Ab scoring prediction analysis.** The BEAM-Ab antigen-library will be used to computationally generate a BEAM Score, using an automated CellRanger software (10X Genomics), which is a measure of antigen-reactivity to identify HIV-1 Env-reactive BCRs. The generation of BEAM Scores use the target antigen barcodes and the control no-antigen barcodes; a positive score is an indication of a higher ratio of antigen binding relative to the control no-antigen conjugate, and is scaled per antigen on a range of 0–100 (lowest to highest Ag-reactivity). BEAM scoring uses beta distribution modeling that computes 100 times the probability that a BCR is binding to an antigen with 92.5% confidence, thus 100 is the maximal BEAM score for the best binding BCRs and as the BEAM score decreases so does the likelihood for BCR binding.

From our pilot BEAM experiment (Fig. S4), we established our working criteria for selection of BCRs from BEAM-Ab for Ab expression to be as follows: BEAM score  $\geq 32$ , UMIs (heavy/light chain genes)  $\geq 3$  (consistent with recommendations from 10X genomics), and UMIs per antigen barcode  $\geq 100$  for IgG BCRs. Using these criteria, we found that 75% of predicted HIV-1 Env-reactive IgG BCRs bound recombinant HIV-1 Env trimers when expressed as mAbs. Moreover, the HIV-1 Env-reactive BCRs identified that matched our scoring criteria did not have a positive BEAM Score  $>1$  for the non-relevant NTD protein. Ongoing studies will optimize BEAM-Ab technology to improve the prediction criteria for mAb binding. We hypothesize that differences in BCR density, and avidity and affinity for binding antigens, will affect the success rates from BCR prediction to actual mAb binding; the impact of these factors on BEAM-Ab pipeline need further evaluation. Moreover, we found BCRs with positive BEAM scores  $<1$  for one antigen that had a positive score  $>32$  for additional antigens, and the IgG mAb bound all the antigens used in the BEAM experiment. These data suggested that antigen proximity to the B cells or differences in antigen avidity or affinity for the BCRs can influence the BEAM scores when multiple antigens are included in the antigen panel. We also found evidence of No-antigen BEAM Assemblies binding to HIV-1 Env trimer-reactive mAb PGT151, suggestive of possible cross-reactivity by this negative control to candidate Env-reactive BCRs as indicated by low level UMIs associated with No-antigen BEAM Assembly for BCRs detected. We speculated that this potential cross-reactivity effect of the No-antigen BEAM Assemblies may have impacted our recovery of candidate BCRs where we relied on BCR Scores to guide selection of mAbs; i.e., following background subtraction using No-antigen BEAM Assembly scores, candidate antigen-reactive BCRs may have been removed because of high levels of No-antigen BEAM Assembly binding that is not significantly lower than binding to a BEAM Assembly that contains a HIV-1 Env antigen. Thus, future studies will also optimize negative controls for background subtraction in our BEAM-Ab pipeline.

**NSEM analysis of mAbs.** To form the antibody-Env complex, 60  $\mu\text{g}$  of either DH1518.1 or DH1518.2 IgG mAb was mixed with 20  $\mu\text{g}$  of T250 Env trimer (T250-4CHIMSOSIPV5.2.8\_avi-Bio/293 F) and brought to 50  $\mu\text{l}$  final volume by addition of buffer containing 20 mM HEPES, pH 7.4, 150 mM  $\text{Na}_2\text{SO}_4$ , 2.5 mM NaCl and 5 mM  $\text{NaN}_3$  (HBSO4-buffer) and incubated at 4 °C overnight. The following day the mixture was separated by FPLC on a Superose 6 Increase 10/300 size-exclusion column. Running buffer contained phosphate-buffered saline with 500 mM  $\text{Na}_2\text{SO}_4$  added. Fractions eluting around 14 ml were collected, pooled and concentrated with 150-kDa MWCO spin concentrators.

Concentrated fractions were then diluted to 0.3 mg/ml nominal SOSIP concentration with HBSO4-buffer augmented with 8 mM glutaraldehyde and incubated 5 min, after which sufficient 1 M Tris buffer, pH 7.4, was added for a final Tris concentration of 80 mM to quench excess glutaraldehyde. Quenched samples were then applied to a glow-discharged carbon-coated EM grid for 10–12 s, blotted, stained with 2 g/dL uranyl formate for 1 min, blotted and air-dried. Grids were examined on a Philips EM420 electron microscope operating at 120 kV and nominal magnification of 49,000 $\times$ , and  $\sim 100$  images were collected on a 76 Mpix CCD camera at 2.4 Å/pixel. Images were analyzed and 3D reconstructions calculated using standard protocols with Relion 3.0<sup>99</sup>. Figures were produced with UCSF Chimera<sup>100</sup>.

Despite similar levels of ELISA binding to the autologous and heterologous HIV-1 Env trimers by the DH1518 mAbs (Fig. 4C), we found that DH1518 mAbs neutralized heterologous tier 2 HIV strains and not the autologous strain (Table S3), suggestive of differences in binding affinities to these Envs that were not detected in ELISA. In fact, our attempts to complex these mAbs with the autologous trimer yielded insufficient particles to get a 3D structure for confirmation via NSEM. Thus, to increase our chances of complex formation for structural analysis, we studied these mAbs in complex with the heterologous Env trimer from the virus that these mAbs neutralized.

**Viral-env RNA sequencing.** We amplified SHIV 3' half genomes from plasma samples of RMs using the well-established single genome sequencing (SGS) method<sup>27</sup>. Briefly, viral RNA was extracted from plasma using QIAamp Viral RNA kit (Qiagen) and reverse transcribed using SuperScript III Reverse Transcriptase (Invitrogen). Viral cDNA was then endpoint diluted and amplified using nested PCR with the kit-based primers<sup>27</sup>. We were able to successfully amplify viral cDNA from plasma samples with viral load of  $\geq 3$  Logs viral RNA copies/ml, consistent with viral cDNA amplification in majority of the neonatal RMs with higher viral loads (Fig. 1)<sup>29</sup>. The sequences were visualized using computational tools as described in the methods for Env signature analysis.

**Eukaryotic cell lines.** We obtained Expi293i cells from ThermoFisher to express recombinant antibodies. TZM-bl cells for HIV neutralization assays were provided by the NIH AIDS Reagent Program. 293 T/17 cells used to generate HIV pseudoviruses for neutralization assays were provided by the American Type Culture Collection (ATCC). Expi293 and TZM-bl cell lines obtained from ThermoFisher and NIH HIV reagent program are provided with a certificate of analysis. Cell identity is verified by morphology or fluorescent markers expressed. Expi293 cell lines used for antibody production undergo mycoplasma testing every 60 days. TZM-bl and 293 T/17 cell lines undergo baseline mycoplasma testing as well as testing at passage 26 ( $\pm 2$ ) and at the end of their cycle which is either 60 passages or 5 months in culture.

**Env signature analysis.** Common sites of variability across HIV-1 *env* in infants are identified using the pipeline “Longitudinal Antigenic Sequences and Sites from Intra-Host Evolution” or LASSIE<sup>64</sup>. Briefly, for each animal, we first identified all sites at which the frequency of the corresponding residue in the SHIV challenge CH848 10.17 DT.E169K was less than 50% within at least one longitudinal time point. We then ranked all sites based on how many times they were shared across multiple animals. Fisher's exact tests were used to test the association with HIV-1 neutralization breadth, given our criteria for development of breadth at 30% of viruses tested, for all sites shared across three or more animals, where breadth was defined as neutralization of 30% of more viruses at the month 18 time point. Logo plots were created using the LANL tool AnalyzeAlign [<https://www.hiv.lanl.gov>]. Env glycan analysis was performed using the LANL tools Glycan Shield Mapping and N-Glycosite [<https://www.hiv.lanl.gov>]. Hamming distances across all sequence pairs were defined as the number of distinct amino acid differences between the two strains, divided by the amino acid



sequence length. Differences in mean Hamming distances were tested using 1-sided Wilcoxon tests. All statistical tests, graphs, and coding were done on the R platform [<http://www.R-project.org>].

### Statistical analysis

For comparison of frequencies, we used Mann Whitney Tests performed in GraphPad Prism software (Fig. 5) and Fishers Exact Test in SAS 9.4 (SAS Institute, Cary, NC) (Fig. 3). Paired Wilcoxon and ANOVA tests were performed in R using the lme4 package for comparisons across groups (Fig. 2 and S12).

The chi-square test or KS test short for the Kolmogorov-Smirnov test was used to separately compare the distribution of mutated heavy, light chain genes, and HCDR3 distribution across the groups. The chi-square statistic and D statistic correspond to *p*-values. The bigger these statistics the smaller the *p*-values. Since the *p*-values of the distributions are very small, the output is just labeled as  $<2.2\text{e-}16$  for all the cases. Thus, the chi-square statistic and D statistic were reported instead. The smaller chi-squared statistic or D statistic is indicative of a smaller difference in groups compared (Table S6).

Area under the curve (AUC) of log transformed viral loads and sequence Hamming distances were computed in R and compared using 2-sided paired Wilcoxon tests (Figs. 1, 8 and S1). Additional testing to account for covariate adjustments (such as viral load) was also performed in R using random effect generalized model regressions available from the lme4 package (Table S7). Dam/neonate pair IDs were used as random effects and dichotomous dam/neonate labels were used as independent variables. Viral loads at specific sampling times were included for viral load-adjusted models.

For Fig. 7C, the extrema of the black lines, the “whiskers”: upper whisker – the minimum of the largest value of the data \*OR\* the 75th percentile +  $1.5 \times$  (75th percentile – 25th percentile – the IQR or interquartile range). Lower whisker – the maximum of the largest value of the data \*OR\* the 25th percentile –  $1.5 \times$  (the IQR or interquartile range).

For the source data of Fig. 6B, C, the raw *p*-values from the two-sided Wald test were used for differential gene expression. These values were not been adjusted for multiple testing. For adjusted *p*-value of each gene, in the context of DESeq2, this was the *p*-value after adjustment for multiple testing, using the Benjamini–Hochberg procedure which controls the false discovery rate (FDR).

### Reporting summary

Further information on research design is available in the Nature Portfolio Reporting Summary linked to this article.

### Data availability

The data presented in this manuscript, and research materials used in this study are available from Duke University upon request and subsequent execution of an appropriate materials transfer agreement. Further information and requests for resources and reagents should be directed to and will be fulfilled by the corresponding author, Wilton B. Williams (wilton.williams@duke.edu). The bulk RNA-sequencing data generated in this study have been deposited in the NCBI Bioproject Database under bioproject ID [PRJNA1077358](https://www.ncbi.nlm.nih.gov/bioproject/PRJNA1077358). The processed bulk RNA-sequencing data generated in this study are provided in the Supplementary Information/Source Data file. The nucleotide sequences for mAbs were provided in the supplemental materials. The source data underlying Figs. 1C, 2A, 2B, 4B, 4C, 4E, 4G, 5 and S7, 6A, B, 6B, 6C, 7A, 7B, 7C, 8C, 8D, 8E, S2A, S2B, S3A, S3B, S3C, S4B, S4C, S8, S8A, S9, S10, and S11 are provided as a Source Data file. Source data are provided with this paper.

### Code availability

Custom scripts used for NGS analysis of Ig genes can be found at <https://zenodo.org/records/11550281>.

## References

- Adkins, B., Leclerc, C. & Marshall-Clarke, S. Neonatal adaptive immunity comes of age. *Nat. Rev. Immunol.* **4**, 553–564 (2004). PubMed PMID: 15229474.
- Semmes, E. C. et al. Understanding early-life adaptive immunity to guide interventions for pediatric health. *Front Immunol.* **11**, 595297 (2021).
- Thome, J. J. et al. Early-life compartmentalization of human T cell differentiation and regulatory function in mucosal and lymphoid tissues. *Nat. Med.* **22**, 72–77 (2016).
- Martinez, D. R., Permar, S. R. & Fouda, G. G. Contrasting adult and infant immune responses to HIV infection and vaccination. *Clin. Vaccin. Immunol.* **23**, 84–94 (2015).
- Hodgins, D. C. & Shewen, P. E. Vaccination of neonates: problem and issues. *Vaccine* **30**, 1541–1559 (2012).
- Marchant, A. & Goldman, M. T cell-mediated immune responses in human newborns: ready to learn? *Clin. Exp. Immunol.* **141**, 10–18 (2005).
- Muenchhoff, M. et al. Nonprogressing HIV-infected children share fundamental immunological features of nonpathogenic SIV infection. *Sci. Transl. Med.* **8**, 358ra125 (2016).
- Han, Q. et al. HIV DNA-adenovirus multiclade envelope vaccine induces Gp41 antibody immunodominance in Rhesus Macaques. *J. Virol.* <https://doi.org/10.1128/JVI.00923-17> (2017).
- Fouda, G. G. et al. Infant HIV Type 1 gp120 vaccination elicits robust and durable anti-V1V2 immunoglobulin G responses and only rare envelope-specific immunoglobulin A responses. *J. Infect. Dis.* **211**, 508–517 (2015).
- Zhang, J., Silvestri, N., Whitton, J. L. & Hasset, D. E. Neonates mount robust and protective adult-like CD8(+) T-cell responses to DNA vaccines. *J. Virol.* **76**, 11911–11919 (2002).
- Ota, M. O. et al. Hepatitis B immunisation induces higher antibody and memory Th2 responses in new-borns than in adults. *Vaccine* **22**, 511–519 (2004).
- Haynes, B. F. & Burton, D. R. Developing an HIV vaccine. *Science* **355**, 1129–1130 (2017).
- Haynes, B. F., Burton, D. R. & Mascola, J. R. Multiple roles for HIV broadly neutralizing antibodies. *Sci. Transl. Med.* **11**, <https://doi.org/10.1126/scitranslmed.aaz2686> (2019).
- Sok, D. & Burton, D. R. Recent progress in broadly neutralizing antibodies to HIV. *Nat. Immunol.* **19**, 1179–1188 (2018).
- Williams, W. B., Wiehe, K., Saunders, K. O. & Haynes, B. F. Strategies for induction of HIV-1 envelope-reactive broadly neutralizing antibodies. *J. Int. AIDS Soc.* **24**, e25831 (2021).
- Hraber, P. et al. Prevalence of broadly neutralizing antibody responses during chronic HIV-1 infection. *AIDS* **28**, 163–169 (2014).
- Goo, L., Chohan, V., Nduati, R. & Overbaugh, J. Early development of broadly neutralizing antibodies in HIV-1-infected infants. *Nat. Med.* **20**, 655–658 (2014).
- Simonich, C. A. et al. HIV-1 neutralizing antibodies with limited hypermutation from an infant. *Cell* **166**, 77–87 (2016).
- Victoria, G. D. et al. Germinal center dynamics revealed by multi-photon microscopy with a photoactivatable fluorescent reporter. *Cell* **143**, 592–605 (2010).
- Victoria, G. D. & Nussenzweig, M. C. Germinal centers. *Annu. Rev. Immunol.* **30**, 429–457 (2012).
- Moody, M. A. et al. Immune perturbations in HIV-1-infected individuals who make broadly neutralizing antibodies. *Sci. Immunol.* **1**, aag0851 (2016).
- Yamamoto, T. et al. Quality and quantity of TFH cells are critical for broad antibody development in SHIVAD8 infection. *Sci. Transl. Med.* **7**, 298ra120 (2015).
- Chowdhury, A. et al. Decreased T follicular regulatory Cell/T follicular helper cell (TFH) in simian immunodeficiency virus-infected



- Rhesus Macaques may contribute to accumulation of TFH in chronic infection. *J. Immunol.* **195**, 3237–3247 (2015).
24. Crotty, S. A brief history of T cell help to B cells. *Nat. Rev. Immunol.* **15**, 185–189 (2015).
  25. Crotty, S. T follicular helper cell differentiation, function, and roles in disease. *Immunity* **41**, 529–542 (2014).
  26. Li, H. et al. Envelope residue 375 substitutions in simian-human immunodeficiency viruses enhance CD4 binding and replication in rhesus macaques. *Proc. Natl Acad. Sci. USA.* **113**, E3413–E3422 (2016).
  27. Li H., et al. New SHIVs and improved design strategy for modeling HIV-1 transmission, immunopathogenesis, prevention and cure. *J. Virol.* <https://doi.org/10.1128/JVI.00071-21> (2021).
  28. Roark, R. S. et al. Recapitulation of HIV-1 Env-antibody coevolution in macaques leading to neutralization breadth. *Science* <https://doi.org/10.1126/science.abd2638> (2020).
  29. Hora, B. et al. Neonatal SHIV infection in rhesus macaques elicited heterologous HIV-1-neutralizing antibodies. *Cell Rep.* **42**, 112255 (2023).
  30. Evangelous, T. D. et al. Host immunity associated with spontaneous suppression of viremia in therapy-naïve young rhesus macaques following neonatal SHIV infection. *J. Virol.* **97**, e0109423 (2023).
  31. Nelson, A. N. et al. Simian-human immunodeficiency virus SHIV.CH505-infected infant and adult rhesus macaques exhibit similar env-specific antibody kinetics, despite distinct t-follicular helper and germinal center B cell landscapes. *J. Virol.* **93** (2019).
  32. Moore, P. L., Williamson, C. & Morris, L. Virological features associated with the development of broadly neutralizing antibodies to HIV-1. *Trends Microbiol.* **23**, 204–211 (2015).
  33. Andrabai, R. et al. Identification of common features in prototype broadly neutralizing antibodies to HIV envelope V2 apex to facilitate vaccine design. *Immunity* **43**, 959–973 (2015).
  34. Wiehe, K. et al. Antibody light-chain-restricted recognition of the site of immune pressure in the RV144 HIV-1 vaccine trial is phylogenetically conserved. *Immunity* **41**, 909–918 (2014).
  35. Pollara, J. et al. G. HIV-1 vaccine-induced C1 and V2 Env-specific antibodies synergize for increased antiviral activities. *J. Virol.* **88**, 7715–7726 (2014).
  36. Walker, L. M. et al. Broad and potent neutralizing antibodies from an African donor reveal a new HIV-1 vaccine target. *Science* **326**, 285–289 (2009).
  37. Bonsignori, M. et al. Staged induction of HIV-1 glycan-dependent broadly neutralizing antibodies. *Sci. Transl. Med.* **9** (2017).
  38. Wagh, K. et al. Completeness of HIV-1 envelope glycan shield at transmission determines neutralization breadth. *Cell Rep.* **25**, 893–908.e7 (2018).
  39. Yang, Y. R. et al. Autologous antibody responses to an HIV envelope glycan hole are not easily broadened in rabbits. *J. Virol.* **94** (2020).
  40. deCamp, A. et al. Global panel of HIV-1 Env reference strains for standardized assessments of vaccine-elicited neutralizing antibodies. *J. Virol.* **88**, 2489–2507 (2014).
  41. Gorman, J. et al. Structures of HIV-1 Env V1V2 with broadly neutralizing antibodies reveal commonalities that enable vaccine design. *Nat. Struct. Mol. Biol.* **23**, 81–90 (2016).
  42. Seaman, M. S. et al. Tiered categorization of a diverse panel of HIV-1 Env pseudoviruses for assessment of neutralizing antibodies. *J. Virol.* **84**, 1439–1452 (2010).
  43. Haynes, B. F. et al. GM. Strategies for HIV-1 vaccines that induce broadly neutralizing antibodies. *Nat. Rev. Immunol.* <https://doi.org/10.1038/s41577-022-00753-w> (2022).
  44. Roskin, K. M. et al. Aberrant B cell repertoire selection associated with HIV neutralizing antibody breadth. *Nat. Immunol.* **21**, 199–209 (2020).
  45. Bradley, T. et al. RAB11FIP5 expression and altered natural killer cell function are associated with induction of HIV broadly neutralizing antibody responses. *Cell* **175**, 387–99.e17 (2018).
  46. Roeder, J. et al. High-frequency, functional HIV-specific T-follicular helper and regulatory cells are present within germinal centers in children but not adults. *Front Immunol.* **9**, 1975 (2018).
  47. Olin, A. et al. Stereotypic immune system development in newborn children. *Cell* **174**, 1277–92.e14 (2018).
  48. Sage, P. T. & Sharpe, A. H. T follicular regulatory cells in the regulation of B cell responses. *Trends Immunol.* **36**, 410–418 (2015).
  49. Linterman, M. A. et al. Foxp3+ follicular regulatory T cells control the germinal center response. *Nat. Med.* **17**, 975–982 (2011).
  50. Wollenberg, I. et al. Regulation of the germinal center reaction by Foxp3+ follicular regulatory T cells. *J. Immunol.* **187**, 4553–4560 (2011).
  51. Chung, Y. et al. Follicular regulatory T cells expressing Foxp3 and Bcl-6 suppress germinal center reactions. *Nat. Med.* **17**, 983–988 (2011).
  52. Sage, P. T., Francisco, L. M., Carman, C. V. & Sharpe, A. H. The receptor PD-1 controls follicular regulatory T cells in the lymph nodes and blood. *Nat. Immunol.* **14**, 152–161 (2013).
  53. Fontenot, J. D., Gavin, M. A. & Rudensky, A. Y. Foxp3 programs the development and function of CD4+CD25+ regulatory T cells. *Nat. Immunol.* **4**, 330–336 (2003).
  54. Hori, S., Nomura, T. & Sakaguchi, S. Control of regulatory T cell development by the transcription factor Foxp3. *Science* **299**, 1057–1061 (2003).
  55. Allan, S. E., Song-Zhao, G. X., Abraham, T., McMurchy, A. N. & Levings, M. K. Inducible reprogramming of human T cells into Treg cells by a conditionally active form of FOXP3. *Eur. J. Immunol.* **38**, 3282–3289 (2008).
  56. Chinen, T. et al. An essential role for the IL-2 receptor in T. *Nat. Immunol.* **17**, 1322–1333 (2016).
  57. Bayer, A. L., Lee, J. Y., de la Barrera, A., Surh, C. D. & Malek, T. R. A function for IL-7R for CD4+CD25+Foxp3+ T regulatory cells. *J. Immunol.* **181**, 225–234 (2008).
  58. Rapp, M. et al. CCL22 controls immunity by promoting regulatory T cell communication with dendritic cells in lymph nodes. *J. Exp. Med.* **216**, 1170–1181 (2019).
  59. Wang, Z. et al. Treg depletion in non-human primates using a novel diphtheria toxin-based anti-human CCR4 immunotoxin. *Mol. Oncol.* **10**, 553–565 (2016).
  60. Alt, F. W. et al. VDJ recombination. *Immunol. Today* **13**, 306–314 (1992).
  61. Schatz, D. G. V(D)J recombination. *Immunol. Rev.* **200**, 5–11 (2004).
  62. Ramesh, A. et al. Structure and diversity of the Rhesus Macaque immunoglobulin Loci through multiple. *Front Immunol.* **8**, 1407 (2017).
  63. Sundling, C. et al. Single-cell and deep sequencing of IgG-switched macaque B cells reveal a diverse Ig repertoire following immunization. *J. Immunol.* **192**, 3637–3644 (2014).
  64. Hraber, P. et al. Longitudinal antigenic sequences and sites from intra-host evolution (LASSIE) identifies immune-selected HIV variants. *Viruses* **7**, 5443–5475 (2015).
  65. Bricault, C. A. et al. HIV-1 neutralizing antibody signatures and application to epitope-targeted vaccine design. *Cell Host Microbe* **25**, 59–72.e8 (2019).
  66. Saunders, K. O. et al. Targeted selection of HIV-specific antibody mutations by engineering B cell maturation. *Science* **366** (2019).
  67. Henderson, R. et al. Structural basis for breadth development in the HIV-1 V3-glycan targeting DH270 antibody clonal lineage. *Nat. Commun.* **14**, 2782 (2023).
  68. Ditse, Z. et al. HIV-1 Subtype C-infected children with exceptional neutralization breadth exhibit polyclonal responses targeting

- known epitopes. *J. Virol.* **92**. <https://doi.org/10.1128/JVI.00878-18> (2018).
69. Williams, W. B. et al. Fab-dimerized glycan-reactive antibodies are a structural category of natural antibodies. *Cell* <https://doi.org/10.1016/j.cell.2021.04.042> (2021).
  70. Moody, M. A. et al. Strain-specific V3 and CD4 binding site autologous HIV-1 neutralizing antibodies select neutralization-resistant viruses. *Cell Host Microbe* **18**, 354–362 (2015).
  71. Williams, W. B. et al. Initiation of HIV neutralizing B cell lineages with sequential envelope immunizations. *Nat. Commun.* **8**, 1732 (2017).
  72. Liao, H. X. et al. Program NCS. Co-evolution of a broadly neutralizing HIV-1 antibody and founder virus. *Nature* **496**, 469–476 (2013).
  73. Gao, F. et al. Cooperation of B cell lineages in induction of HIV-1 broadly neutralizing antibodies. *Cell* **158**, 481–491 (2014).
  74. Doria-Rose, N. A. et al. Program NCS. Developmental pathway for potent V1V2-directed HIV-neutralizing antibodies. *Nature* **509**, 55–62 (2014).
  75. Haynes, B. F., Kelsoe, G., Harrison, S. C. & Kepler, T. B. B-cell-lineage immunogen design in vaccine development with HIV-1 as a case study. *Nat. Biotechnol.* **30**, 423–433 (2012).
  76. Dahmer, M. K., Cornell, T. & Quasney, M. W. Genetic and epigenetic factors in the regulation of the immune response. *Curr. Opin. Pediatr.* **28**, 281–286 (2016).
  77. Wiehe, K. et al. Functional relevance of improbable antibody mutations for HIV broadly neutralizing antibody development. *Cell Host Microbe* **23**, 759–65.e6 (2018).
  78. Mothé, B. R. et al. Expression of the major histocompatibility complex Class I molecule Mamu-A\*01 is associated with control of simian immunodeficiency virus SIVmac239 replication. *J. Virol.* **77**, 2736–2740 (2003).
  79. Yant, L. J. et al. DI. The high-frequency major histocompatibility complex Class I allele Mamu-B\*17 is associated with control of simian immunodeficiency virus SIVmac239 replication. *J. Virol.* **80**, 5074–5077 (2006).
  80. Loffredo, J. T. et al. Mamu-B\*08-positive macaques control simian immunodeficiency virus replication. *J. Virol.* **81**, 8827–8832 (2007).
  81. Egan, M. A. et al. Use of major histocompatibility complex class I/peptide/beta2M tetramers to quantitate CD8(+) cytotoxic T lymphocytes specific for dominant and nondominant viral epitopes in simian-human immunodeficiency virus-infected rhesus monkeys. *J. Virol.* **73**, 5466–5472 (1999).
  82. Abel, K. The rhesus macaque pediatric SIV infection model - a valuable tool in understanding infant HIV-1 pathogenesis and for designing pediatric HIV-1 prevention strategies. *Curr. HIV Res.* **7**, 2–11 (2009).
  83. Hessel, A. J. et al. Early short-term treatment with neutralizing human monoclonal antibodies halts SHIV infection in infant macaques. *Nat. Med.* **22**, 362–368 (2016).
  84. Jaworski, J. P. et al. Neutralizing polyclonal IgG present during acute infection prevents rapid disease onset in simian-human immunodeficiency virus SHIVSF162P3-infected infant rhesus macaques. *J. Virol.* **87**, 10447–10459 (2013).
  85. Saunders, K. O. et al. Vaccine induction of CD4-mimicking HIV-1 broadly neutralizing antibody precursors in macaques. *Cell* **187**, 79–94.e24 (2024).
  86. Li, D. et al. In vitro and in vivo functions of SARS-CoV-2 infection-enhancing and neutralizing antibodies. *Cell* **184**, 4203–19.e32 (2021).
  87. Alam, S. M. et al. Antigenicity and immunogenicity of RV144 vaccine AIDSVAX clade E envelope immunogen is enhanced by a gp120 N-terminal deletion. *J. Virol.* **87**, 1554–1568 (2013).
  88. Saunders, K. O. et al. Vaccine elicitation of high mannose-dependent neutralizing antibodies against the V3-Glycan broadly neutralizing epitope in nonhuman primates. *Cell Rep.* **18**, 2175–2188 (2017).
  89. Liao, H. X. et al. Vaccine induction of antibodies against a structurally heterogeneous site of immune pressure within HIV-1 envelope protein variable regions 1 and 2. *Immunity* **38**, 176–186 (2013).
  90. Liao, H. X. et al. Initial antibodies binding to HIV-1 gp41 in acutely infected subjects are polyreactive and highly mutated. *J. Exp. Med.* **208**, 2237–2249 (2011).
  91. Montefiori, D. C. Measuring HIV neutralization in a luciferase reporter gene assay. *Methods Mol. Biol.* **485**, 395–405 (2009).
  92. Kechin, A., Boyarskikh, U., Kel, A. & Filipenko, M. cutPrimers: a new tool for accurate cutting of primers from reads of targeted next generation sequencing. *J. Comput. Biol.* **24**, 1138–1143 (2017).
  93. Kersey, P. J. et al. Ensembl Genomes: an integrative resource for genome-scale data from non-vertebrate species. *Nucleic Acids Res.* **40**, D91–D97 (2012).
  94. Dobin, A. et al. STAR: ultrafast universal RNA-seq aligner. *Bioinformatics* **29**, 15–21 (2013).
  95. Anders, S., Pyl, P. T. & Huber, W. HTSeq—a Python framework to work with high-throughput sequencing data. *Bioinformatics* **31**, 166–169 (2015).
  96. Love, M. I., Huber, W. & Anders, S. Moderated estimation of fold change and dispersion for RNA-seq data with DESeq2. *Genome Biol.* **15**, 550 (2014).
  97. Huber, W. et al. Orchestrating high-throughput genomic analysis with Bioconductor. *Nat. Methods* **12**, 115–121 (2015).
  98. Subramanian, A. et al. Gene set enrichment analysis: a knowledge-based approach for interpreting genome-wide expression profiles. *Proc. Natl Acad. Sci. USA.* **102**, 15545–15550 (2005).
  99. Zivanov, J. et al. New tools for automated high-resolution cryo-EM structure determination in RELION-3. *Elife* **7** <https://doi.org/10.7554/eLife.42166> (2018).
  100. Pettersen, E. F. et al. UCSF Chimera—a visualization system for exploratory research and analysis. *J. Comput. Chem.* **25**, 1605–1612 (2004).

## Acknowledgements

We thank the Duke Human Vaccine Institute (DHVI) finance and program management teams for their invaluable administrative support: Kimberly Kobes, Cindy Bowman, Whitney Beck, and Amanda Newman. We would like to thank the following individuals for technical support, including plasmid preparation and sequencing for expression of recombinant antibodies, cell preparation for antibody expression, western blot QC of antibodies, and managing the inventories of antibodies and envelope proteins described in this study: Esther Lee, Alecia Brown, Rebecca M. Williams, Mary Tess Overton, Savanna Toure, Joena Bal, Katrina Hodges, and Lena Smith. We would like to thank Roman Fenner for contributing to data collation from our collaborators. Animals were housed and cared for at BIOQUAL Inc. by a team of expert technicians and veterinary staff. Thanks to Georgeanna Morton and Sampa Santra at Beth Israel Deaconess Medical Center, Harvard School of Medicine, Boston, MA, for animal genotyping. The DHVI Accessioning Unit provided support for sample processing, storage and distribution. BEAM-Ab and bulk-RNA sequencing were done in collaboration with the DHVI Viral Genetics Analysis core facility. We thank 10X Genomics (Pleasanton, CA) team members for consultation with development of our single cell assays, including BEAM-Ab: Bryan Hess, Nirav Patel and Ryan Mote. We thank the Takara Bio (San Jose, CA, USA) product management team on immune profiling for providing a customized kit, and the Bioinformatics R&D team for analytical support, for macaque Ig gene sequencing; Shuwen Chen, Shaveta Goyal, Jason Whitham, and Mike Covington. This work was funded by NIH, NIAID R01-AI140897 and Duke University School of Medicine Whitehead Scholarship (W.B.W.), NIAID Contract

#HHSN272201800004C (X.S., D.C.M.), and NIH R01 AI160607(G.M.S.). This publication was made possible with help from the Duke University Center for AIDS Research (CFAR), an NIH funded program (5P30 AI064518). We are grateful for key resources provided by the Director of DHVI, Dr. Barton Haynes.

## Author contributions

Statement. W.B.W. conceived and designed the study, evaluated all data, and wrote and edited the paper. S.H. performed binding serology assays, collated and reviewed all the data, and edited the paper. H.L., A.S. and G.M.S. designed and/or performed viral Env evolution studies and analyses. X.S., M.S.S. and D.C.M. performed neutralization assays. M.M. performed hook production in BEAM-Ab, expressed recombinant mAbs, and performed binding assays for plasma and mAbs. R.T. performed cell staining for flow sorting in BEAM-Ab and immune cell phenotyping assays. Y.C. performed library amplification for BEAM-Ab, bulk RNA-seq studies, Illumina NGS studies, and sequenced all libraries. B.H., T.D.E. and J.T.C. contributed to BEAM-Ab assay development. K.We., H.F.K., M.B., E.V.I, S.V., and J.M.B. conducted sequencing analyses. K.M. and R.J.E. performed structural studies. E.E.G. and K.Wa. performed statistical analyses and analyzed envelope sequences for mutation signatures and viral diversity. C.K., T.G., and M.A.M. coordinated sample processing, storage and distribution. T.DeM., N.DN. and T.N.D. performed viral load testing. N.S., J.M. and M.G.L. designed and conducted animal studies. K.O.S provided key reagents. Y.W. provided statistical support.

## Competing interests

The authors declare no competing interests.

## Additional information

**Supplementary information** The online version contains Supplementary Material available at <https://doi.org/10.1038/s41467-024-54753-6>.

**Correspondence** and requests for materials should be addressed to Wilton B. Williams.

**Peer review information** *Nature Communications* thanks the anonymous reviewers for their contribution to the peer review of this work. A peer review file is available.

**Reprints and permissions information** is available at <http://www.nature.com/reprints>

**Publisher's note** Springer Nature remains neutral with regard to jurisdictional claims in published maps and institutional affiliations.

**Open Access** This article is licensed under a Creative Commons Attribution-NonCommercial-NoDerivatives 4.0 International License, which permits any non-commercial use, sharing, distribution and reproduction in any medium or format, as long as you give appropriate credit to the original author(s) and the source, provide a link to the Creative Commons licence, and indicate if you modified the licensed material. You do not have permission under this licence to share adapted material derived from this article or parts of it. The images or other third party material in this article are included in the article's Creative Commons licence, unless indicated otherwise in a credit line to the material. If material is not included in the article's Creative Commons licence and your intended use is not permitted by statutory regulation or exceeds the permitted use, you will need to obtain permission directly from the copyright holder. To view a copy of this licence, visit <http://creativecommons.org/licenses/by-nc-nd/4.0/>.

© The Author(s) 2024

<sup>1</sup>Duke Human Vaccine Institute, Duke University School of Medicine, Durham, NC, USA. <sup>2</sup>Departments of Medicine and Microbiology, Perelman School of Medicine, University of Pennsylvania, Philadelphia, PA, USA. <sup>3</sup>Department of Surgery, Duke University School of Medicine, Durham, NC, USA. <sup>4</sup>Fred Hutchinson Cancer Center, Seattle, WA, USA. <sup>5</sup>Department of Integrative Immunobiology, Duke University School of Medicine, Durham, NC, USA. <sup>6</sup>Department of Pediatrics, Duke University School of Medicine, Durham, NC, USA. <sup>7</sup>Department of Medicine, Duke University School of Medicine, Durham, NC, USA. <sup>8</sup>Los Alamos National Laboratory, Los Alamos, NM, USA. <sup>9</sup>Beth Israel Deaconess Medical Center, Harvard Medical School, Boston, MA, USA. <sup>10</sup>Department of Molecular Genetics and Microbiology, Duke University School of Medicine, Durham, NC, USA. <sup>11</sup>BIOQUAL Inc., Rockville, MD, USA. <sup>12</sup>Present address: Department of Medicine, Duke University School of Medicine, Durham, NC, USA. <sup>13</sup>These authors contributed equally: Sommer Holmes, Hui Li, Xiaoying Shen, Mitchell Martin, Ryan Tuck, Yue Chen. ✉ e-mail: [wilton.williams@duke.edu](mailto:wilton.williams@duke.edu)